

1 **High peatland methane emissions following permafrost thaw: enhanced acetoclastic**
2 **methanogenesis during early successional stages**

3 Liam Heffernan^{1,2*}★, Maria A. Cavaco^{3*}★, Maya P. Bhatia³, Cristian Estop-Aragonés⁴,
4 Klaus-Holger Knorr⁴, David Olefeldt¹

5
6 ¹ Department of Renewable Resources, University of Alberta, Edmonton, AB T6G 2H1,
7 Canada. ² Evolutionary Biology Centre, Department of Ecology and Genetics/Limnology,
8 Uppsala University, Norbyvägen 18D, 752 36, Uppsala, Sweden. ³ Department of Earth and
9 Atmospheric Sciences, University of Alberta, Edmonton, AB T6G 2H1, Canada. ⁴ Institute of
10 Landscape Ecology, Ecohydrology and Biogeochemistry Group, University of Münster,
11 Münster, Germany

12 *Corresponding authors: Liam Heffernan (liam.heffernan@ebc.uu.se) and Maria A. Cavaco
13 (cavaco@ualberta.ca)

14 ★ These authors contributed equally to this work

15
16
17
18
19
20
21
22
23

24 **Abstract**

25 Permafrost thaw in northern peatlands often leads to increased methane (CH₄) emissions, but
26 the underlying controls responsible for increased emissions and the duration for which they
27 persist have yet to be fully elucidated. We assessed how shifting environmental conditions
28 affect microbial communities, and the magnitude and stable isotopic signature ($\delta^{13}\text{C}$) of CH₄
29 emissions along a thermokarst bog transect in boreal western Canada. Thermokarst bogs
30 develop following permafrost thaw when dry, elevated peat plateaus collapse and become
31 saturated and dominated by *Sphagnum* mosses. We differentiated between a young and a
32 mature thermokarst bog stage (~30 and ~200 years since thaw, respectively). The young bog
33 located along the thermokarst edge, was wetter, warmer and dominated by hydrophilic
34 vegetation compared to the mature bog. Using high throughput 16S rRNA gene sequencing,
35 we show that microbial communities were distinct near the surface and converged with depth,
36 but lesser differences remained down to the lowest depth (160 cm). Microbial community
37 analysis and $\delta^{13}\text{C}$ data from CH₄ surface emissions and dissolved gas depth profiles show that
38 hydrogenotrophic methanogenesis was the dominant pathway at both sites. However, mean
39 $\delta^{13}\text{C}$ -CH₄ signatures of both dissolved gases profiles and surface CH₄ emissions were found
40 to be isotopically heavier in the young bog (-63 ‰ and -65 ‰, respectively) compared to the
41 mature bog (-69 ‰ and -75 ‰, respectively), suggesting that acetoclastic methanogenesis
42 was relatively more enhanced throughout the young bog peat profile. Furthermore, mean
43 young bog CH₄ emissions of 82 mg CH₄ m⁻² day⁻¹, were ~ three times greater than the 32 mg
44 CH₄ m⁻² day⁻¹, observed in the mature bog. Our study suggests that interactions between the
45 methanogenic community, hydrophilic vegetation, warmer temperatures, and saturated
46 surface conditions enhance CH₄ emissions in young thermokarst bogs, but that these
47 favorable conditions only persist for the initial decades after permafrost thaw.

48

49 **Keywords**

50 Permafrost, peatland, thermokarst, 16S RNA, isotope, methanogenesis, microbial
51 community, methane emissions

52 **1. Introduction**

53 Methane (CH₄) emissions in northern peatlands are typically thought to be driven by
54 environmental and ecological conditions such as temperature, water table position, and
55 vegetation community (Bellisario et al., 1999). However, CH₄ emissions are ultimately the
56 result of microbial activity and understanding the interactions between environmental
57 conditions and microbial processes is key to understanding the impact of disturbances on
58 peatland CH₄ emissions. Increased disturbances such as permafrost thaw are transforming
59 northern latitude peatlands (Helbig, Pappas & Sonnentag, 2016), through the disruption of the
60 frozen landscape and environmental conditions responsible for the regional accumulation of
61 large peatland carbon (C) stores. Rapidly rising northern air temperatures (Mudryk et al.,
62 2018) are predicted to lead to widespread gradual thawing of permafrost (Schaefer et al.,
63 2011) and subsequent thermokarst development in high C density permafrost peatlands
64 (Olefeldt et al., 2016). Thermokarst formation in ice-rich permafrost peatlands is
65 characterized by ground subsidence and surface inundation (Camill, 1999). This exposes
66 previously frozen C to anaerobic microbial decomposition and potential mineralization into
67 greenhouse gases (Schuur et al., 2015). Redox conditions following thermokarst formation
68 are an important control of decomposition, with 3 – 4 times greater C mineralization
69 occurring as aerobic respiration compared to anaerobic respiration (Schädel et al., 2016).
70 Increased emissions of methane (CH₄) due to thermokarst formation are projected to result in
71 a positive feedback with climate warming (Turetsky et al., 2020). However, the magnitude of
72 peatland CH₄ emissions and the metabolic pathways responsible for these emissions in

73 response to permafrost thaw remain uncertain, as does the period for which these conditions
74 and emissions persist.

75 Methanogenesis, conducted by methanogenic archaea belonging to phylum
76 Euryarchaeota, is one of the most prominent microbial processes contributing to the
77 anaerobic decomposition of organic matter in water-logged permafrost soils (Cai et al., 2016;
78 Knoblauch et al., 2018). Methanogenesis occurs primarily via two pathways: acetoclastic
79 methanogenesis and hydrogenotrophic methanogenesis (Whiticar et al., 1986; Whiticar,
80 1999). Acetoclastic methanogenesis involves the cleavage of acetate into CH₄ and CO₂ and
81 when considering these two species, causes less apparent fractionation than the
82 hydrogenotrophic methanogenesis pathway. This results in acetoclastic methanogenesis
83 yielding comparatively isotopically heavy δ¹³C-CH₄ (δ¹³C = -65 to -50‰). The reduction of
84 CO₂ and H₂ in hydrogenotrophic methanogenesis typically produces CH₄ lighter in ¹³C (δ¹³C
85 = -110 to -60‰) (Hornibrook et al., 1997, 2000). While the two pathways are
86 stoichiometrically equal (Conrad, 1999; Corbett et al., 2013), the activity of acetoclastic and
87 hydrogenotrophic methanogens are governed by different extrinsic controls (Bridgham et al.,
88 2013).

89 Hydrogenotrophic methanogenesis is thought to be the main pathway of CH₄
90 formation in northern peatlands (Hornibrook et al., 1997; Galand et al., 2005). However, the
91 acetoclastic pathway can dominate in the upper layers of more minerotrophic, nutrient rich
92 peatlands (Popp et al., 1999; Chasar et al., 2000) where there are sufficient levels of acetate
93 (Ye et al., 2012). During the initial decades following thaw, surface runoff of nutrients from
94 surrounding intact peat plateaus (Keuper et al., 2012; 2017) and increased connectivity to
95 regional hydrology (Connon et al., 2014), can result in more minerotrophic conditions. Such
96 shifts in hydrology, temperature, nutrients, redox conditions, and vegetation communities
97 following permafrost thaw have been shown to increase the prevalence of acetoclastic

98 methanogenesis and CH₄ emissions (Hodgkins et al., 2014; McCalley et al., 2014). However,
99 this potential post-thaw enhancement of acetoclastic methanogenesis needs to be considered
100 in context of the existing methanogenic community that developed in the peat profile before
101 thaw. For example, historical environmental conditions have been shown to have a legacy
102 effect on the methanogenic community following thaw and can therefore be a key constraint
103 on methanogenic community structure and activity post-thaw (Holm et al., 2020; Lee et al.,
104 2012). Overall, an understanding of the methanogenic community's response following thaw
105 to shifts in both surface conditions and exposure to previously frozen organic matter is key to
106 estimating CH₄ emissions from thermokarst peatlands.

107 Environmental conditions following permafrost thaw in peatlands are characterized
108 by a drastic shift in water table position and increased wetness, increased soil temperatures,
109 and a change in vegetation community associated with increased labile inputs (Beilman,
110 2001; Burd et al., 2020; Camill, 1999). These shifts may provide optimal conditions for CH₄
111 production and emissions, particularly in the initial decades following thaw. Peatland CH₄
112 emissions are constrained by water table position (Huang et al., 2021; Strack et al., 2004),
113 and surface inundation leads to increased CH₄ emissions (Tuittila et al., 2000). Methane
114 production and emissions are positively influenced by soil temperatures (Hopple et al., 2020;
115 Olefeldt et al., 2017), and peatland CH₄ emissions have been shown to increase when both
116 water table position and temperatures are high (Grant, 2015). The colonization of vegetation
117 associated with fresh, labile inputs has also been shown to increase both the magnitude and
118 temperature sensitivity of CH₄ emissions in peatlands (Leroy et al., 2017; McNicol et al.,
119 2019). As such, many studies have focussed on the relationship between water table position,
120 soil temperature and vegetation communities in determining CH₄ fluxes following thaw
121 (Johnston et al., 2014; Turetsky et al., 2007; Wickland et al., 2006). However, while these
122 environmental conditions are key drivers of CH₄ emissions, they are unable to fully account

123 for the variability in permafrost peatland CH₄ emissions (Juottonen et al., 2021; Kuhn et al.,
124 2021). Some of this unaccounted variance may be in part explained by microbial activity, as
125 changes in the composition and abundance of methanogenic community members can
126 contribute significantly towards peatland CH₄ emissions (Fritze et al., 2021). Relatively few
127 studies have assessed how shifts in environmental conditions and ensuing changes in
128 methanogenic community structure influences CH₄ emissions following thaw (McCalley et
129 al., 2014), an interaction that may be significant both at the local and circumpolar scale.

130 In this study we assess the impact of permafrost thaw on peatland methanogenic
131 community composition and CH₄ emissions along a space-for-time thaw gradient that
132 includes an intact peat plateau and an adjacent thermokarst bog with areas that have thawed
133 ~30 and ~200 years ago (herein referred to as young bog and mature bog, respectively).
134 Thermokarst formation has resulted in distinct environmental conditions at each stage along
135 this thaw gradient. We herein define these distinct environmental conditions as water table
136 position and surface wetness, soil temperatures, and vegetation community. Along this
137 gradient we assessed methanogenic community structure down to 160 cm. We hypothesize
138 that: (1) shifting environmental conditions along the permafrost thaw gradient results in a
139 successional microbial community and a restructuring of the methanogenic community, and
140 (2) the warmer conditions and hydrophilic vegetation community in the young bog, along
141 with the exposure of previously frozen peat, will result in a greater relative abundance of
142 acetoclastic methanogens throughout the depth profile, and subsequently greater overall CH₄
143 emissions. In the young bog and mature bog, we measured the concentration and $\delta^{13}\text{C}$ -
144 signature of dissolved CH₄ and CO₂ down to 245 cm, and the rates and $\delta^{13}\text{C}$ -signature of both
145 CH₄ and CO₂ land-atmosphere fluxes. The combined approach of measuring dissolved gas
146 depth profiles and surface emissions, in tandem with assessing the structure of the
147 methanogenic community along a depth profile, allows us to determine how changing

148 environmental conditions following thaw impacts methanogenic pathways and community
149 composition. Utilizing this approach, we can subsequently gain further insight into how long
150 elevated surface CH₄ emissions may persist post-thaw. Furthermore, this approach highlights
151 that while environmental conditions are important in determining CH₄ emissions, microbial
152 community composition, and changes in the methanogenic community structure are likely to
153 significantly influence CH₄ emissions following thaw.

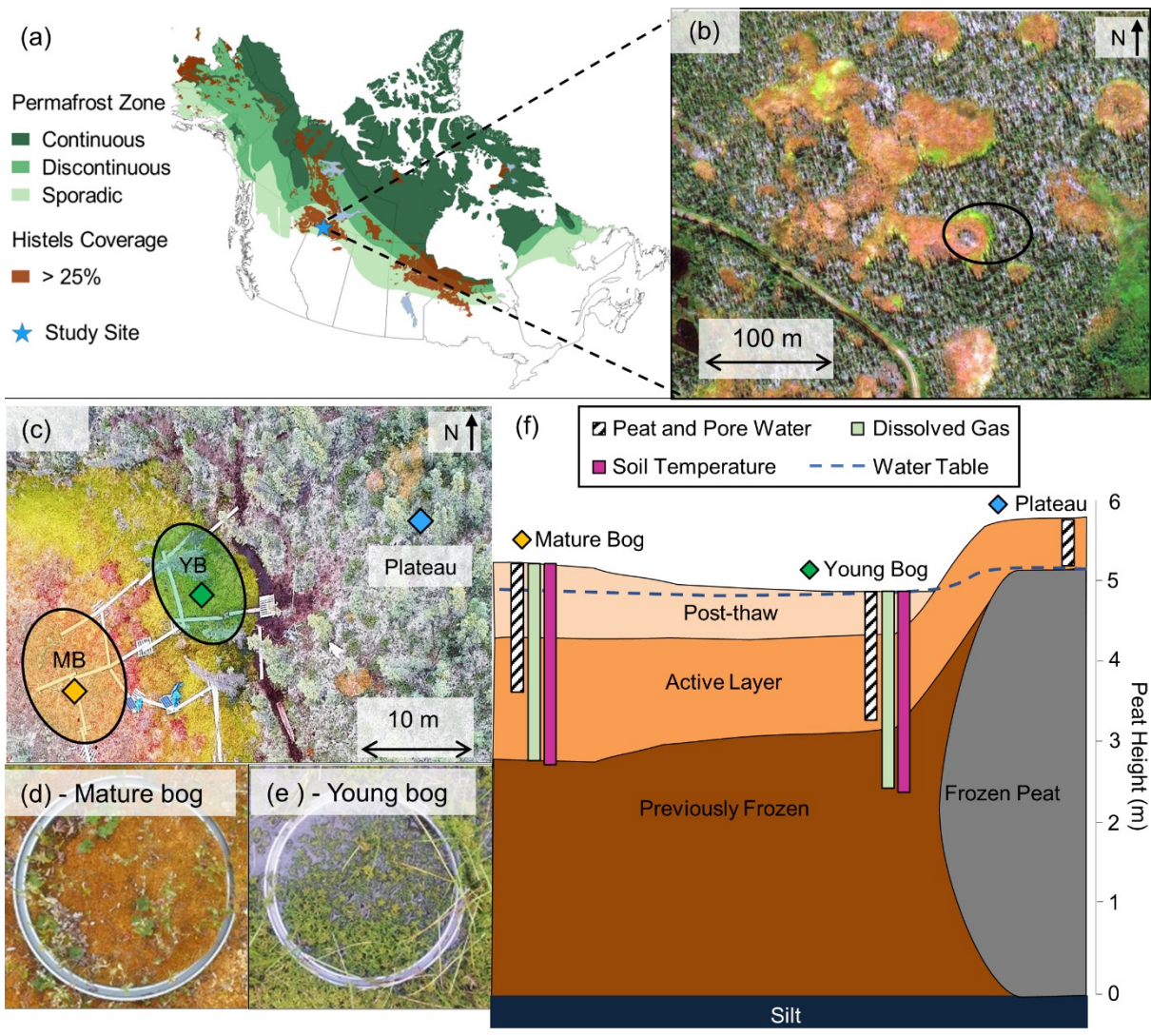
154 **2. Methods**

155 *2.1 Study Site and Design*

156 The Lutose peatland study site (59.5°N, 117.2°W; Figure 1) is located on the Interior
157 Plains of western Canada, within the zone of discontinuous permafrost (Brown et al., 1997;
158 Heginbottom et al., 1995). The climate is continental with a monthly average summer high
159 temperature of 16.1 °C (July), winter low of -22.8 °C (January), and annual average air
160 temperature of -1.8 °C (Climate-Data.org, 2019 – data from site located ~50 km south of
161 Lutose). Annual average precipitation is 391 mm, of which three quarters fall as rain between
162 May and September. In the discontinuous permafrost zone of the Interior Plains in boreal
163 western Canada, ~40% of the landscape is covered by permafrost peatlands that have
164 between 2 and 6 m deep peat deposits (Gibson et al., 2018; Vitt et al., 2000). The peatland
165 complexes in this area are a fine-scale mosaic of permafrost peat plateaus, and permafrost-
166 free ponds, fens, and bogs (Zoltai, 1993; Bauer et al., 2003; Vitt et al., 2000; Pelletier et al.,
167 2017), and they are similar to those found in the Hudson Bay Lowlands (Kuhry, 2008) and
168 Alaska (Jones et al., 2017). The Lutose peatland complex is representative of the peatlands
169 found in the discontinuous permafrost zone of the Interior Plains in western Canada
170 (Heffernan et al., 2020). The site has 5 – 6 m deep peat and has transitioned through multiple
171 developmental stages since it began accumulating organic matter ~8,800 years ago. It

172 transitioned from a marsh, through a fen and a bog stage prior to permafrost aggradation
 173 ~1,800 years ago (Heffernan et al., 2020). Peatlands in the Interior Plains in western Canada
 174 are one of the three largest stores of organic carbon found in peatlands within the permafrost
 175 zone, the other two being the Hudson Bay Lowlands and the West Siberian Lowlands
 176 (Hugelius et al., 2020; Olefeldt et al., 2021). Within the sporadic and discontinuous
 177 permafrost zone of our study region >15% of the total peat plateau area has thawed and
 178 formed thermokarst bogs in the last 30 years (Baltzer et al., 2014; Gibson et al., 2018).
 179 Projections for this area suggests total permafrost lost from plateaus by 2050 (Chasmer and
 180 Hopkins, 2017).

181



182

183 **Figure 1.** Lutose peatland site location and study design. (a) Site location (Lutose, Alberta,
184 Canada 59.5°N, 117.2°W) in boreal western Canada. Green shading represents permafrost
185 zonation (Brown et al., 1997) and brown shading represents areas with >25% permafrost
186 peatland (histels) extent (Hugelius et al., 2014). (b) Geoeye satellite image of study site
187 (image from <https://zoom.earth/>), 0.46 m resolution. Circle represents the area where
188 sampling took place. (c) Aerial image of study transect, locations of peat and dissolved gas
189 sampling in the plateau (blue diamond), young bog (green diamond), and mature bog (orange
190 diamond), and area where collars for gas flux measurements were located in the young bog
191 (YB, green) and mature bog (MB, orange) (Aerial photo credit: Olefeldt, David). (d, e)
192 Surface vegetation in the mature bog and young bog (f) Soil profile of thaw transect based on
193 (Heffernan et al., 2020). The transition to Post-thaw peat occurs at 29 cm and 71 cm in the
194 young bog and mature bog respectively. Peat (core) and pore water (pore water peepers),
195 including microbial community, sampling depth profile 0 – 160 cm shown as white column
196 with diagonal black lines. Dissolved gas (diffusive samplers) sampling depth profile 0 – 245
197 cm shown as light green column. Soil temperature depth profile 0 – 250 cm shown as purple
198 column. Average water table depth shown as dashed blue line.

199

200 The studied transect represents a space-for-time gradient of permafrost thaw that includes
201 three thaw stages: a permafrost peat plateau, and a young (~30 years since thaw) and mature
202 (~200 years since thaw) part of an adjacent thermokarst bog. The timing of permafrost thaw
203 was previously determined by ¹⁴C dating the shift in macrofossil vegetation indicative of
204 thaw, at 29 cm in the young bog and at 71 cm in the mature bog (Figure 1f) (Heffernan et al.,
205 2020). The peat plateau has an active layer thickness of ~70 cm and its surface is raised 1 – 2
206 m above the adjacent thermokarst bog due to the presence of excess ground ice, resulting in
207 relatively dry surface conditions where the water table generally follows the deepening of the
208 seasonally thawed peat layer (Zoltai, 1972). This thaw stage is characterized by a stunted,
209 open black spruce (*Picea mariana*) canopy and ground cover of lichens (*Cladonia* spp.),
210 *Sphagnum fuscum* hummocks, and low-lying ericaceous shrubs as is characteristic of the peat
211 plateaus in the area (Vitt et al., 1994). The young bog stage is narrow (<5 – 10 m wide) and is
212 located next to the actively thawing area of the peat plateau. The young bog has an average
213 growing season water table position of 1.3 ± 4.9 cm below the peat surface. These inundated
214 conditions result in the dominance of a hydrophilic vegetation community (Figure 1e)
215 consisting of *Sphagnum riparium*, bog-sedge (*Carex limosa*), and rannoch rush (*Scheuchzeria*

216 *palustris*). The mature bog is ~10 – 15 m from the young bog and is drier, compared to the
217 young bog, with an average growing season water table position of 22.9 ± 9.3 cm below the
218 surface. The dominant vegetation reflects these drier conditions and consists of *Sphagnum*
219 *fuscum*, *Sphagnum magellanicum*, leather leaf (*Chamaedaphne calyculata*), cloudberry
220 (*Rubus chamaemorus*), *Eriophorum vaginatum* tussocks, and some black spruce (*Picea*
221 *mariana*) regrowth (Figure 1d). The mature bog is located >10 – 20 m from the thawing
222 plateau edge.

223 2.2 Site Preparation and Monitoring of Environmental Conditions

224 The Lutose peatland study site was established in 2015 and a boardwalk was constructed
225 to minimize disturbances along the peat plateau - thermokarst bog transect. Three collars for
226 surface greenhouse gas flux (39 cm diameter) measurements were permanently installed to
227 a depth of 20 cm in both the young and mature thermokarst bog stages. The top of each collar
228 was aligned with the peat surface. PVC wells (2 cm diameter) were installed directly next to
229 each collar and were used to manually monitor the water table position during each gas flux
230 measurement. We monitored soil temperature (°C) at 10, 30, 50, 75, 100, 150, 200, and 250
231 cm every 30 min from May – September 2018 using permanently installed loggers (Hobo 8k
232 Pendant Onset Computer, Bourne, MA, USA) in both thermokarst bog stages. Temperature
233 depth profiles were established centrally among collars in each thermokarst bog stage, in
234 areas that had similar vegetation, water table position, and distance from the thawing edge as
235 the collars.

236 Custom made plexiglass pore water suction (Heffernan et al., 2021) and diffusive
237 equilibration gas sampling devices (Knorr et al., 2009) were installed in July 2016 in the
238 young and mature bog. These devices were installed in both thermokarst bog stages ~1 m
239 from the nearest flux measurement collar. Pore water suction devices were installed to a

240 depth of 160 cm and consisted of 15 sampling depths, with each sampling depth connected to
241 the surface via silicone tubing. This allowed for repeated non-destructive pore water
242 sampling. Three diffusive gas sampling devices were installed in each thermokarst bog stage,
243 where two collected dissolved soil gas samples from 5 – 95 cm deep and a third from 115 –
244 245 cm. Each diffusive gas sampler consisted of a PVC pipe with a 10 cm long sampling
245 section centred at each sampling depth. Sampling sections consisted of ~2 m of silicon tubing
246 (3 mm i.d., 5 mm o.d.) wrapped around the PVC pipe and kept in place by PVC-spacers at
247 the top and bottom of each interval. Silicone tubes were sealed at one end whereas the other
248 end was connected to polyurethane tubing (1.8 mm i.d.) that ran back up inside the PVC tube
249 to reach the peat surface where it was sealed with a three-way stopcock. Silicone tubing has
250 been shown to be permeable to gases such as CO₂ and CH₄ within a number of hours, while
251 remaining impermeable to water, making it suitable for sampling of dissolved soil gases
252 (Kammann et al., 2001).

253 *2.3 Pore water chemistry and peat enzyme activity*

254 Pore water dissolved organic matter (DOM) chemistry and peat enzyme activity
255 presented in this study have previously been published (Heffernan et al., 2021), and are
256 briefly described here. Pore water samples for DOM chemistry were taken monthly from
257 May – September 2018 using the previously described pore water suction devices in the
258 young bog and mature bog. Three 60 mL samples were taken from all 15 measurement
259 depths by applying a vacuum at the surface and collecting water with syringes via a three-
260 way stopcock. Each water sample was immediately filtered through 0.7 µm pore size glass
261 fiber filters (GF/F Whatman) into two acid-washed amber glass bottles, with one sample
262 acidified with 0.6 mL 2N HCl to prevent further microbial activity. Pore water samples were
263 transported in a cooled container and stored at 4 °C prior to analysis. Pore water DOM was

264 analyzed for pH, phosphate (PO_4^{3-} ; $\mu\text{g L}^{-1}$), dissolved organic carbon (DOC; mg L^{-1}), total
265 dissolved nitrogen (TDN; mg L^{-1}) concentrations, phenolic contents, specific UV absorbance
266 at 254 nm (SUVA, $\text{L mg C}^{-1} \text{m}^{-1}$; Weishaar et al., 2003) and spectral slope between 250 – 465
267 nm ($S_{250-465}$, nm^{-1} ; Helms et al., 2008). SUVA and $S_{250-465}$ values are used to indicate
268 aromaticity, with high SUVA indicating a high aromatic content and lower $S_{250-465}$
269 indicating low molecular weight and decreasing aromaticity (Hansen et al., 2016).

270 Peat cores extracted to a depth of 160 cm were stored at 4 °C for less than one week in the
271 laboratory before homogenization to determine potential soil enzyme activities. We
272 performed hydrolytic enzyme assays for four enzymes; phosphatase, β -N-glucosaminidase, β -
273 glucosidase, and β -cellobiosidase using fluorogenic 4-methylumbelliferone labelled
274 substrates (Dunn et al., 2014). We assayed oxidative enzyme activity by measuring laccase
275 activity using syringaldazine (Criquet et al., 2000; Jassey et al., 2012). We summarized the
276 activity of all enzymes using a multi-functionality index based on z-scores (Allan et al., 2015;
277 Heffernan et al., 2021).

278 *2.4 Surface Land-Atmosphere Gas Fluxes*

279 We measured surface land-atmosphere greenhouse gas fluxes (CH_4 and carbon dioxide;
280 CO_2) monthly from May – September 2018 at the 3 collars in each peatland stage using the
281 static chamber method (Carroll & Crill, 1997). The chamber used to capture land-atmosphere
282 fluxes was a transparent cylindrical Plexiglass chamber with a basal area of 0.12 m^2 , height
283 of 0.40 m, and volume of 47.8 L. The chamber was equipped with three fans (Micronel
284 Ventilator D341T012GK-2, BEDEK GmbH, Dinkelsbühl, Germany) to mix air during
285 measurements and a temperature sensor (Hobo RH Smart Sensor, S-THB-M002, Onset
286 computers, Bourne, USA) that was shaded from direct sunlight (Burger et al., 2016). An
287 airtight seal was formed between the chamber and collar by pouring water in a $\sim 1.5 \text{ cm}$ deep
288 well around the upper circumference of each collar. Land-atmosphere fluxes of CO_2

289 (ecosystem respiration) and CH₄ were captured simultaneously in darkened conditions by
290 covering the chamber with a reflective shroud. Gas concentrations were determined at a
291 temporal resolution of 1 s using an Ultraportable Greenhouse Gas Analyser (Los Gatos
292 Research, CA, USA) and real-time fluxes were monitored using the VNV® Viewer
293 (RealVNC® Limited, UK) application with an iPad mini 2 (Apple Inc.).

294 The rates of CH₄ and CO₂ land-atmosphere fluxes (*Flux*) were calculated using the ideal
295 gas law following:

$$296 \quad Flux = slope \frac{P.V}{R.T.A} \quad (1)$$

297 where slope is the linear rate of change of gas concentration (μmol mol⁻¹ second⁻¹) over the
298 measurement period inside the chamber; P is an atmospheric pressure (atm) constant of 0.96
299 atm; V is chamber volume (L); R is the universal gas constant (L atm K⁻¹ mol⁻¹); T is the
300 average temperature (K) inside the chamber during the measurement; and A is the chamber
301 basal area (m²). Chamber closure for each flux measurement was 5 minutes with the first 2
302 minutes discarded to ensure fluxes (i.e., change in concentration over time) with $R^2 > 0.75$.
303 We report CO₂ fluxes in g CO₂ m⁻² day⁻¹ and CH₄ fluxes in mg CH₄ m⁻² day⁻¹, with positive
304 values indicating fluxes to the atmosphere. To quantify the proportion of C being emitted as
305 CH₄, we standardized our CO₂ and CH₄ fluxes per g C emitted. The proportion of C emitted
306 as CH₄ (CH₄:C emissions) was calculated as

$$307 \quad CH_4:C \text{ emissions} = \frac{CH_4 \text{ m}^{-2} \text{ day}^{-1}}{CH_4 \text{ m}^{-2} \text{ day}^{-1} + CO_2 \text{ m}^{-2} \text{ day}^{-1}} \quad (2)$$

308 2.5 δ¹³C-signature of CH₄ emissions

309 We assessed the δ¹³C-CO₂ and δ¹³C-CH₄ signatures of ecosystem respiration (CO₂) and
310 CH₄ emissions. This was done similarly to regular measurements of CO₂ and CH₄ fluxes, but
311 using a smaller, opaque chamber of 31.1 L and discrete syringe-samples for δ¹³C analysis in

312 combination with the continuous monitoring of gas concentrations described above. Gas
313 syringe samples were taken using a 20 mL syringe via a three-way stopcock placed between
314 the sealed chamber and gas inlet port on the Ultraportable Greenhouse Gas Analyser. Gas
315 samples were then injected into a 37.5 mL sealed glass-vial that had been flushed with
316 nitrogen gas prior to sealing. Chamber enclosure time ranged from 30 – 50 minutes with 4 – 5
317 samples being taken during this time. Samples were taken either every 10-minutes or once a
318 minimum change in CO₂ (30 μmol mol⁻¹) and CH₄ (1 μmol mol⁻¹) concentrations was
319 observed. An atmospheric gas sample was used as a time-zero measurement when assessing
320 the change in concentration over time. Glass-vials containing samples were stored at 4 °C
321 until analysis. These measurements were taken in September and October 2016 from 1 collar
322 in both the young and mature bog, with each collar measured twice.

323 We measured the δ¹³C values of gas samples from both the chamber fluxes and
324 atmospheric background. To assess whether the gas concentration of each sample fit within
325 the measurement range required for δ¹³C analysis we measured CO₂ and CH₄ concentrations
326 using 1 – 3 mL from each vial. Following these concentration measurements, the remaining
327 sample (17 – 19 ml) was diluted with nitrogen gas to a final volume of 20 mL and injected
328 into a Small Sample Introduction Module (SSIM, Picarro, California, USA) system to
329 measure δ¹³C signatures. The δ¹³C-CO₂ and δ¹³C-CH₄ signature was measured in-line with a
330 cavity ring-down spectrometer (G2201-L, Picarro, California, USA) that had been calibrated
331 using certified standards.

332 We then used the time-series of δ¹³C-CH₄ and CH₄ concentrations to estimate the δ¹³C-
333 CH₄ signature of the CH₄ released to the atmosphere using Keeling plots (Keeling, 1958).
334 Using this approach, the δ¹³C-CH₄ signature of gas in each sample is plotted on the y-axis
335 against the inverse of CH₄ gas concentrations (1/[CH₄]). The y-axis intercept of the linear
336 regression represents the mean isotopic signature of the CH₄ source (Fisher et al., 2017).

337 While fractionation during diffusive transport may influence these estimates, it has been
338 shown in similar systems to be of minor importance compared to other contributing processes
339 (Preuss et al., 2013; Nielsen et al., 2019).

340 *2.6 Dissolved gas depth profiles*

341 Dissolved gas samples were collected using diffusive equilibration gas sampling
342 devices. Samples were taken from the following 15 depths: every 10 cm down to 95 cm
343 starting at 5 – 15 cm, and then at 115 cm, 140 cm, 165 cm, 195 cm, and 245 cm. Once a
344 month from May – September 2018 a ~7 mL gas sample was drawn from each depth using a
345 10 mL plastic syringe. These gas samples were immediately injected into a 10 mL sealed
346 glass-vial that had been flushed with nitrogen gas prior to sealing, and then were stored at 4
347 °C until analysis. A total of 214 CO₂ and 211 CH₄ dissolved gas concentration measurements
348 were made by injecting 1 – 3 mL of gas into a gas chromatograph with an FID and CO₂
349 methanizer (8610C Gas Chromatograph, SRI Instruments, California, USA). We measured
350 $\delta^{13}\text{C-CO}_2$ and $\delta^{13}\text{C-CH}_4$ signatures using the previously mentioned cavity ringdown
351 spectrometer and SSIM system. As with surface chamber gas samples, dissolved gas samples
352 were diluted with N₂ to 20 ml. However, dissolved gas concentrations were considerably
353 higher than gas concentrations found in the surface chambers, and some were well above the
354 optimal concentration range required for accurate $\delta^{13}\text{C}$ analysis for the SSIM system even
355 after dilution. To fit within measurement range of the system, further dilution resulted in CO₂
356 concentrations below detectable limits. As such, we were able to obtain 90 and 75
357 measurements of $\delta^{13}\text{C-CH}_4$ in the young and mature bog, respectively, and 93 measurements
358 of $\delta^{13}\text{C-CO}_2$ in both.

359 We used the $\delta^{13}\text{C-CO}_2$ and $\delta^{13}\text{C-CH}_4$ signature of each gas sample to calculate the
360 apparent fraction factor α_c , where $\alpha_c = [^{13}\text{C-CO}_2 + 1000]/[^{13}\text{C-CH}_4 + 1000]$. The α_c can serve

361 as an isotopic indicator of the pathway of methanogenesis, with typical values of 1.060 –
362 1.090 observed for hydrogenotrophic methanogenesis and 1.040 – 1.060 for acetoclastic
363 methanogenesis (Chanton et al., 2005).

364 *2.7 Peat and pore water sample collection for microbial community composition* 365 *analyses*

366 Microbial community composition was characterized in both peat and peat pore water
367 samples from depths between 0 – 160 cm in the young bog and mature bog. Focusing on peat
368 samples, microbial community composition in the active layer of the peat plateau was
369 assessed from depths between 0 – 30 cm. Peat cores were extracted in June and September
370 2018. Near-surface cores were extracted using a cutting tool to 30 cm deep in the peat plateau
371 and young bog, and 50 cm deep in the mature bog. Surface cores were limited to 30 cm in the
372 plateau due to the presence of ground ice during sampling in June. Surface core depths
373 differed between the young bog and mature bog due to differences in the water table position.
374 Deeper core sections (down to 160 cm) in the young bog and mature bog were extracted
375 using a Russian peat corer (4.5 cm inner-diameter, Eijkelkamp, Giesbeek, The Netherlands).
376 Cores were extracted from two boreholes located ~20 cm apart, alternating between
377 boreholes to avoid disturbance contamination from the 10 cm corer tip during the coring
378 process. To do so, 50 cm long core sections were taken alternatively from each borehole, with
379 each core having a 10 cm overlap with the previous core taken from the adjacent borehole. In
380 the field, immediately after the entire core was extracted, cores were divided into 15
381 subsections. The first two subsections contained peat from 0 – 5 cm and 5 – 10 cm, followed
382 by 10 cm increments down to 120 cm, and two further subsections from 130 – 140 cm and
383 150 – 160 cm. Peat from each interval was sub-sampled using sterilized forceps and placed
384 directly into Whirl-Pak® bags, and frozen within 3 hours of sampling for transportation back

385 to the laboratory. Once samples reached the laboratory, they were frozen at -80 °C until
386 analysis.

387 We also sampled peat pore water at all 15 peat sampling depths in September 2018 from
388 the pre-installed pore water suction sampling devices mentioned above. We extracted 60 mL
389 pore water samples by applying a vacuum at the surface and collecting water with new plastic
390 60 mL syringes. Pore water was immediately filtered through sterile 0.2 µM pore size
391 Polyvinylidene difluoride (PVDF) membrane sterivex filters (MilliporeSigma). Microbial
392 cells were retained on the filter, and remaining porewater in the sterivex was removed via
393 extrusion using a 60 mL sterile syringe. Sterivex filters were then immediately flash-frozen at
394 -80 °C in a liquid nitrogen dry-shipper to preserve microbial community members until
395 analysis could take place.

396 *2.8 DNA extraction*

397 Genomic DNA was extracted from all peat and pore water samples using the DNeasy
398 PowerSoil kit (Qiagen) and the PowerWater DNeasy kit (Qiagen), respectively, to assess the
399 differences in microbial community structure. Extraction of DNA from both sample types
400 was followed as described by the manufacturer (Qiagen), with two modifications: (i) for peat
401 samples, prior to mechanical lysis using bead beating, the prepared samples were chemically
402 lysed by incubation at 70 °C for 10 minutes in the provided lysis solution, and (ii) sterivex
403 (pore water) samples were incubated with rotation at 37 °C following addition of lysis buffer.
404 These modifications were made to increase total DNA yield. The amount of isolated DNA
405 from each sample was then determined using a Qubit fluorometer (model 2.0, using the 1×HS
406 dsDNA kit), with concentrations ranging between ~0.1 and 22.4 ng µL⁻¹. This extracted DNA
407 served as the template for polymerase chain reaction (PCR) analyses described below.

408 *2.9 Sequencing and computational analyses*

409 We amplified 16S rRNA genes using universal prokaryotic primers 515F (Parada,
410 Needham & Fuhrman, 2016) and 926R (Quince et al., 2011). Each primer also contained a
411 six-base index sequence for sample multiplexing (Bartram et al., 2011). The PCR mix (25µL
412 total volume) contained 1 × Q5 reaction buffer, 0.5 µM forward primer, 0.5 µM reverse
413 primer, 200 µM dNTPs, 0.500 U Q5 polymerase (New England Biolabs, Ipswich, M.A.,
414 U.S.A) and 2.5 µL of genomic template. Genomic extracts with DNA concentrations of
415 greater than 2 ng µL⁻¹ were diluted 1:100 in nuclease-free water. The PCR was performed as
416 follows: 95 °C for 3 minutes, 35 cycles of 95 °C for 30 seconds, 60 °C for 30 seconds, 70 °C
417 for 1 minute and a final extension of 70 °C for 10 minutes. Pooled 16S rRNA gene amplicons
418 were purified using Nucleomag beads and a 4.5 pM library containing 50% PhiX Control v3
419 (Illumina, Canada Inc., NB, Canada) was sequenced on a MiSeq instrument (Illumina Inc.,
420 CA, USA) using a 2 × 250 cycle MiSeq Reagent Kit v3 (Illumina Canada Inc) at the
421 Molecular Biology Service Unit (MBSU, University of Alberta). The MiSeq reads were
422 demultiplexed using MiSeq Reporter software version 2.5.0.5. Each read pair was assembled
423 using the paired-end assembler for Illumina sequences (PANDAseq; Masella, Bartram &
424 Truszkowski, 2012) with a quality threshold of 0.9, dictating that 90% of overlapping reverse
425 and forward reads must match in order to assemble reads into read pairs. Assembled reads
426 were analyzed using the Quantitative Insights Into Microbial Ecology II pipeline (QIIME2;
427 Boylen et al., 2020). Sequences were clustered into amplicon sequence variants (ASVs) with
428 chimeric sequences, singletons and low abundance ASVs removed using DADA2 (Callahan
429 et al., 2019). All representative sequences were classified with the Greengenes reference
430 database, using the most recent release (version 13.8; McDonald et al., 2012). Although
431 Greengenes is not updated as frequently as the SILVA database, we chose to use it to classify
432 our ASVs as a comparison of both databases revealed that they captured a similar number of
433 archaea (total of 51187 methanogenic read counts attributed to SILVA *versus* 51141

434 methanogenic read counts attributed to Greengenes). The taxonomic resolution between both
435 databases was also similar, identifying the same kinds of phyla, families and genus, and
436 methanogens (e.g., Methanoregula, Methanosarcinales, etc.). Given these similarities, and the
437 fact that methanogen nomenclature has not changed significantly over time, we ultimately
438 chose to use Greengenes because it was able to resolve more methanogenic families
439 belonging to Methanocelalles and Methanomassiliicoccaceae particularly, compared to
440 SILVA. The Greengenes database is also still commonly used to explore methanogenic
441 archaeal communities in current literature (Vanwonderghem et al., 2016, Lin et al., 2017,
442 Carson et al., 2019). Furthermore, since 1021 methanogenic reads were captured per sample,
443 on average, using Greengenes and are comparable to other studies (Vishnivetskaya et al.,
444 2018; Holm, et al., 2020) we believe that our approach is sufficient for covering methanogen
445 diversity.

446 2.10 Statistical analyses

447 All statistical analyses were carried out in R (Version 3.4.4, R Core Team, 2015) using
448 the *nlme*, *vegan*, *factoextra*, *ggplot2*, *VariancePartition* and *ggpubr* packages (Pinheiro et al.,
449 2017; Oksanen et al., 2013; Kassambara & Mundt, 2017; Wickham, 2016; Hoffman &
450 Schadt, 2016; Kassambara, 2018). For Analysis of Variance (ANOVAs), distribution of the
451 data was inspected visually for normality along with the Shapiro-Wilk test. We tested
452 homogeneity of variances using the *car* package and Levene's test (Fox and Weisberg, 2011).
453 We report uncertainty as ± 1 standard deviation, except for land-atmosphere greenhouse gas
454 fluxes which we report as $\pm 95\%$ confidence intervals. We here define the statistical
455 significance level at 5%.

456 We used ANOVAs and Bonferroni post-hoc tests on linear mixed effects models to
457 address our second hypothesis and to evaluate significant differences and seasonal trends in

458 greenhouse gas fluxes and dissolved gas depth profiles. We performed these tests to assess
459 whether thaw stage (young bog or mature bog) influenced greenhouse gas fluxes and
460 dissolved gas depth profiles. This approach was used to test for significant differences in CH₄
461 fluxes, ratio of CH₄:C emissions, and source ¹³C-CH₄ signature intercepts of Keeling plots
462 between young bog and mature bog stages. In each linear mixed effect model, sampling
463 month and peatland stage were defined as fixed effects whereas sampling collar was defined
464 as a random effect. Similarly, we tested for significant differences between the young and
465 mature bog depth profiles with respect to dissolved CH₄ and CO₂ concentrations, δ¹³C-CH₄
466 and δ¹³C-CO₂ values, α_c values, and pore water chemistry. In these models, sampling month
467 and peatland stage were defined as fixed effects while sample depth was defined as a random
468 effect.

469 Following microbial 16S rRNA gene sequencing, sample reads were rarefied to the
470 lowest read count of 28,129 for all subsequent analyses. These sequences represent whole
471 microbial community data that was used to determine whether there was evidence of changes
472 in microbial community structure representing the successional peatland stages following
473 permafrost thaw throughout the 160 cm depth peat profile. In addition, to address our first
474 hypothesis, we assessed differences in community composition across both peat and pore
475 water and to determine whether seasonality impacted microbial community structure in both
476 sample matrices. Here, Bray Curtis dissimilarity matrices for overall microbial community
477 data were used, at 999 permutations, to identify distinct groupings assessed at the 95%
478 confidence interval in NMDS ordinations. These distinct groupings were further evaluated for
479 significance using the non-parametric permutational analysis of variance (PERMANOVA)
480 test.

481 To further test our first hypothesis, methanogens were selected at the order level from
482 our whole community data using Greengenes-assigned taxonomy. Utilizing their assigned

483 taxonomy, the pathways through which identified methanogens conduct methanogenesis was
484 determined by comparing our findings with the literature (Berghuis et al., 2019; Stams et al,
485 2019; Kendall & Boone, 2006; Zhang et al., 2020). Focusing on the methanogenic
486 community allowed us to specifically assess how permafrost thaw affects the microbial
487 community responsible for CH₄ production and net CH₄ emissions following thaw. We
488 utilized our methanogenic community data to construct redundancy analyses (RDA) and
489 relative abundance bar plots. RDAs were conducted using a Hellinger-transformed
490 methanogenic community. Explanatory variables (i.e., dissolved concentrations of CO₂, CH₄,
491 DOC, temperature, enzymatic activity estimate, thaw stage, depth, and distance to water
492 table) were scaled about the mean. These explanatory variables had variance standardized,
493 were checked for collinearity (parameters with variance inflation value > 10 were removed)
494 and selected for significance using backward selection, set at 1,000 permutations. The
495 significance of the RDA model, and of each axis was tested using ANOVAs, set at 999
496 permutations. Variance partitioning analyses were conducted to assess the contribution of
497 significant environmental parameters (i.e., thaw stage and distance to water table) on the
498 structuring of the Hellinger-transformed methanogenic community. Distance from water table
499 reflects the distance (in cm) a certain sample is from the water table in different stages of
500 thaw (young bog and mature bog). Due to the smaller size of our methanogenic community
501 relative to the total community, and the lack of some data at certain depths, we combined
502 pore water and peat samples together for these analyses. Relative abundance, which measures
503 how common or rare a particular microorganism is relative to the entire microbial
504 community, of methanogenic orders related to acetoclastic or hydrogenotrophic
505 methanogenesis processes were plotted according to depth. Significant differences in
506 methanogenic community composition between depths were assessed using the non-

507 parametric Kruskal-Wallis test with a Benjamini-Hochberg correction for multiple
508 comparisons, after running a Wilcox rank sum test.

509 **3. Results**

510 *3.1 Site environmental conditions*

511 The young bog was wetter and warmer than the mature bog throughout the May –
512 September 2018 study period. In June, following snowmelt, the water table was at its highest
513 at 2.2 ± 0.6 cm above the surface in the young bog. The highest water table position in the
514 mature bog was 17.5 ± 1.9 cm below the peat surface and observed in July. The water table
515 dropped during the season and in September was 5.7 ± 2.2 cm and 27.3 ± 1.2 cm below the
516 peat surface, in the young bog and mature bog respectively. In the plateau, the seasonally
517 thawed layer gradually deepened during the growing season, with an active layer depth of
518 79.5 ± 13.7 cm measured in September. The water table in the peat plateau followed the
519 deepening of the seasonally thawed layer.

520 Soil temperatures followed the seasonal climate but were dampened and had temporal
521 lags in deeper peat layers (Figure S1a). The highest young bog and mature bog soil
522 temperatures at 10 cm depth occurred in July, at 14.3 and 14.1 °C, respectively. At 100 cm
523 depth the maximum temperatures occurred in August and September, at 8.6 and 6.9 °C,
524 respectively for the young and mature bog. Soil temperatures at 250 cm were still rising at the
525 end of September, peaking at 4.1 and 3.2 °C in the young bog and mature, respectively. The
526 young bog was consistently warmer than the mature bog throughout the study by on average
527 0.9 ± 0.9 °C, 1.8 ± 1.0 °C, and 0.5 ± 0.4 °C at 10 cm, 100 cm, and 250 cm depths,
528 respectively.

529 Across all depths and sampling occasions, average pH was higher (ANOVA: $F_{(1, 77)} =$
530 35.2 , $P < 0.001$) in the young bog than in the mature bog at 4.1 ± 0.2 and 3.9 ± 0.2

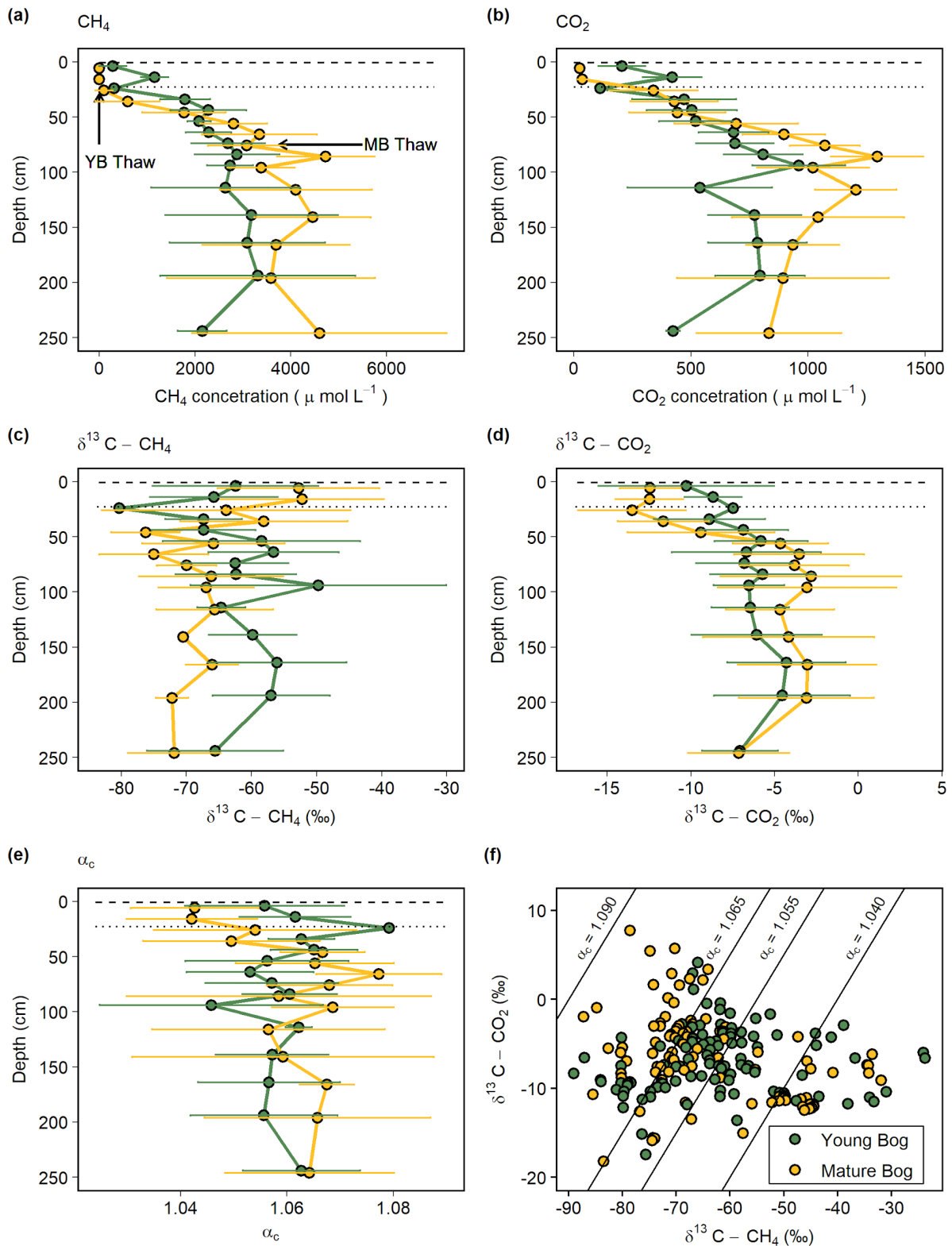
531 respectively. In contrast, DOC at 69.2 ± 18.4 and 53.8 ± 5.4 mg C L⁻¹ (ANOVA: $F_{(1, 82)} =$
532 38.7 , $P < 0.001$) and total dissolved nitrogen at 1.5 ± 1.4 and 0.9 ± 0.1 mg L⁻¹ (ANOVA: $F_{(1,$
533 $82)} = 12.8$, $P < 0.01$) were higher in the mature bog than in the young bog, respectively.
534 Average SUVA values were higher (ANOVA: $F_{(1, 82)} = 103.5$, $P < 0.001$) in the young bog
535 (3.2 ± 0.4 L mg C⁻¹ m⁻¹) compared to the mature bog (2.6 ± 0.4 L mg C⁻¹ m⁻¹), indicating
536 DOM with a greater aromatic content in the young bog. However, average spectral slope
537 ($S_{250-465}$) values were also greater (ANOVA: $F_{(1, 81)} = 6.9$, $P < 0.05$) in the young bog ($-$
538 0.016 ± 0.002 nm⁻¹) compared to the mature bog (-0.017 ± 0.003 nm⁻¹), indicating lower
539 molecular weight and decreasing aromaticity. Average phenolics (0.6 ± 0.2 and 0.6 ± 0.2 mg
540 L⁻¹) and phosphate (PO_4^{3-} : 9.0 ± 14.3 and 6.7 ± 3.0 $\mu\text{g L}^{-1}$) were similar between the young
541 bog and mature bog, respectively, across all depths and sampling occasions. Full details of
542 DOM chemistry results can be found in Heffernan et al., (2021). Of note is the fact that the
543 pore water chemistry was compared across all depths in this study, in contrast to Heffernan et
544 al., (2021) in which pore water found above and below the transition indicating permafrost
545 thaw was compared.

546 *3.2 Concentrations and isotopic signatures of dissolved gases*

547 Dissolved CH₄ increased with depth below the water table in both the young and
548 mature bog (Figure 2a). Dissolved CH₄ concentrations in the young bog increased with depth,
549 from $19 \mu\text{mol L}^{-1}$ at 5 cm depth, to a peak of $5,400 \mu\text{mol L}^{-1}$ at 195 cm. Dissolved CH₄
550 concentrations in the mature bog remained low above the water table ($<6 \mu\text{mol L}^{-1}$ below 25
551 cm), but then increased to $4,100 \pm 1,700 \mu\text{mol L}^{-1}$ between 115 and 250 cm depth and peaked
552 at $6,800 \mu\text{mol L}^{-1}$. Dissolved CO₂ concentrations followed a very similar pattern to CH₄,
553 increasing with depth in both the young and mature bog (Figure 2b). Again, the mature bog
554 had overall higher concentrations, with mean average values ranging from 340 – 1,295 μmol

555 L^{-1} and peaking at $1,500 \mu\text{mol L}^{-1}$ at 85 cm. In contrast, the young bog had average values
 556 ranging from $113 - 960 \mu\text{mol L}^{-1}$ and peaked at $1,200 \mu\text{mol L}^{-1}$ at 95 cm (Figure 2b).

557



558

559 **Figure 2.** Average seasonal (May – September) depth profiles in the young (green, black
560 circles) and mature (yellow, black circles) bog of (a) dissolved CH₄ concentration (μmol L⁻¹),
561 (b) dissolved CO₂ concentration (μmol L⁻¹), (c) δ¹³C-CH₄ (‰), (d) δ¹³C-CO₂ (‰), and (e)
562 apparent fractionation factor (α_c) between dissolved CH₄ and CO₂. (f) Cross-plot of
563 corresponding δ¹³C-CH₄ and δ¹³C-CO₂ values (‰) in the young bog and mature bog, from
564 raw data used in panels (c) and (d). Diagonal lines represent different α_c where α_c 1.040 –
565 1.065 represents acetoclastic methanogenesis, and α_c 1.055 – 1.09 represents
566 hydrogenotrophic methanogenesis (Whiticar, 1999). (a) – (e) Dashed and dotted horizontal
567 lines represent water table depth in the young (YB) and mature bog (MB) respectively.
568 Arrows in panel (a) represent depth of thaw transition in both the young (29 cm) and mature
569 bog (71 cm), i.e., the transition from deep peat (accumulated prior to thawing) and shallow
570 peat (accumulated post thawing).

571

572 The young bog and mature bog had distinct profiles of δ¹³C values for both CH₄ and CO₂
573 (Figure 2c, d). The young bog had no apparent trend with depth for both δ¹³C-CH₄ (ANOVA;
574 F_(14, 45) = 1.75, P = 0.08) and δ¹³C-CO₂ (ANOVA; F_(14, 46) = 1.79, P = 0.07), averaging -62.4
575 ± 7.0 ‰ and -6.8 ± 1.6 ‰, respectively (Figure 2c, d). In the mature bog we observed
576 significant depth trends for both δ¹³C-CH₄ (ANOVA: F_(14, 43) = 3.19, P < 0. 01) and δ¹³C-
577 CO₂ (ANOVA: F_(14, 49) = 6.22, P < 0.001). These significant depth trends are due to
578 isotopically heavy δ¹³C-CH₄ and light δ¹³C-CO₂ above the water table, which suggests an
579 influence from CH₄ oxidation. When comparing δ¹³C depth profiles between the thermokarst
580 bogs we focused on those values taken from under the water table to avoid the effect of CH₄
581 oxidation observed above the water table in the mature bog. Under the water table, δ¹³C-CH₄
582 values in the mature bog were significantly lighter (ANOVA: F_(1, 64) = 18.72, P < 0.001)
583 compared to the young bog at an average of -68.7 ± 5.0 ‰ and -62.4 ± 7.0 ‰, respectively.
584 Conversely, the mature bog had isotopically heavier δ¹³C-CO₂ than the young bog below the
585 water table (ANOVA: F_(1, 71) = 13.86, P < 0.001).

586 The apparent fractionation factor (α_c) is a robust parameter to characterize the relative
587 contribution of CH₄ production pathways, with values of 1.040 – 1.060 indicating
588 acetoclastic methanogenesis and 1.060 – 1.090 for hydrogenotrophic methanogenesis
589 (Chanton et al., 2005). Similar to the gas δ¹³C depth-profiles, we found no clear trend with

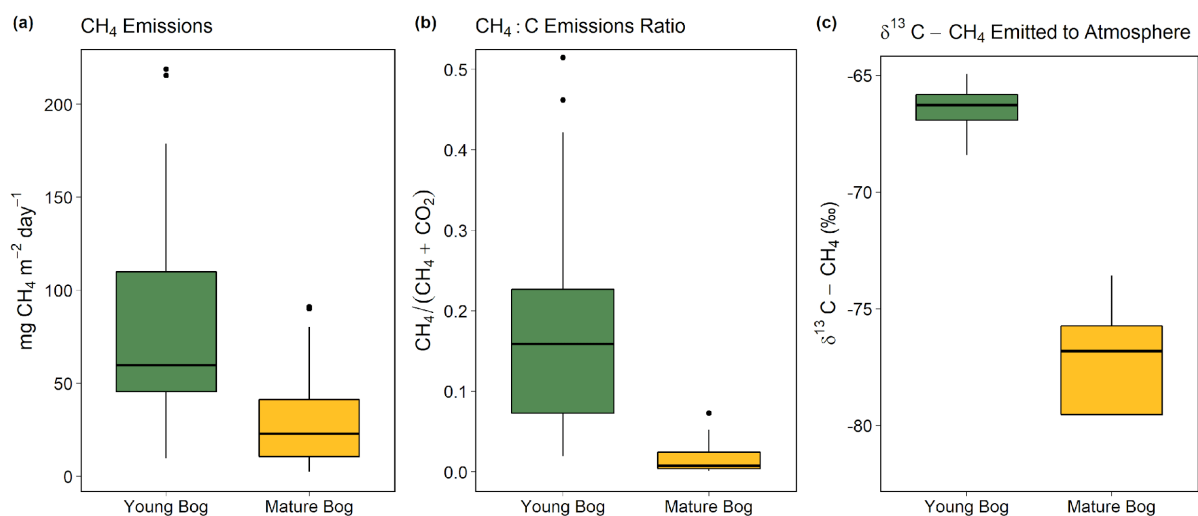
590 depth for α_C values in the young bog (ANOVA; $F_{(14, 44)} = 0.87, P = 0.59$) with an average of
591 1.058 ± 0.012 and range of 1.018 – 1.079 (Figure 2e). In the mature bog, we found a clear
592 depth trend in α_C values (ANOVA: $F_{(14, 43)} = 5.71, P < 0.001$). Similar to the $\delta^{13}C$ depth
593 profiles in the mature bog, this significant depth trend in α_C is due to the influence of CH_4
594 oxidation above the water table, with the lowest α_C values being those from samples collected
595 above the water table at 5, 15, and 25 cm. The average α_C beneath the water table in the
596 mature bog was 1.064 ± 0.017 and ranged from 1.015 – 1.094. When comparing α_C values
597 from beneath the water table between the young and mature bog we found that α_C values were
598 significantly lower in the young bog (ANOVA: $F_{(1, 63)} = 30.8, P < 0.001$).

599 In the isotopic ratio cross-plot of $\delta^{13}C-CH_4$ and $\delta^{13}C-CO_2$ (Figure 2f), most of the young
600 bog had α_C values of between 1.055 – 1.065 (29 in total), with a greater number of samples
601 (21) between $\alpha_C = 1.040$ – 1.055, compared to the mature bog (15). In contrast, a greater
602 proportion of the mature bog samples had $\alpha_C > 1.065$ (42 in the young bog and 52 in the
603 mature bog). There was no clear depth trend in the α_C values and no samples in this study had
604 $\alpha_C > 1.090$. Several samples (13) from the young bog and mature bog had α_C values of $<$
605 1.040, likely due CH_4 oxidation (Knorr et al., 2009).

606 *3.3 Magnitude and isotopic signature of land-atmosphere gas fluxes*

607 The young bog had almost three times greater average CH_4 fluxes than the mature bog
608 during the May – September study period, at 82.3 ± 21.9 mg CH_4 m^{-2} day^{-1} and 30.8 ± 10.6
609 mg CH_4 m^{-2} day^{-1} , respectively (Figure 3a). Fluxes of CH_4 in the young bog were greatest
610 between June and August, ranging from 80.6 ± 40.3 mg CH_4 m^{-2} day^{-1} to 100.9 ± 63.1 mg
611 CH_4 m^{-2} day^{-1} . The lowest young bog CH_4 fluxes were observed in September at 55.0 ± 17.7
612 mg CH_4 m^{-2} day^{-1} (Figure S3a). Mature bog CH_4 fluxes were greatest in September ($55.8 \pm$
613 21.1 mg CH_4 m^{-2} day^{-1}) and lowest in May (5.6 ± 2.7 mg CH_4 m^{-2} day^{-1}). Ecosystem

614 respiration (CO_2 emissions measured with dark chambers) was significantly lower in the
 615 young bog than mature bog, with study period averages of 0.6 ± 0.3 and $1.9 \pm 0.3 \text{ g CO}_2 \text{ m}^{-2}$
 616 day^{-1} , respectively (Figure S3). Maximum ecosystem respiration in the young bog occurred in
 617 August ($1.6 \text{ g CO}_2 \text{ m}^{-2} \text{ day}^{-1}$) and was much lower during the other four months (monthly
 618 averages of 0.2 to $0.4 \text{ g CO}_2 \text{ m}^{-2} \text{ day}^{-1}$). Ecosystem respiration rates in the mature bog were
 619 elevated from June to August (monthly averages between 2.1 and $2.6 \text{ g CO}_2 \text{ m}^{-2} \text{ day}^{-1}$),
 620 and decreased in September ($0.8 \text{ g CO}_2 \text{ m}^{-2} \text{ day}^{-1}$). The proportion of total C emissions (sum
 621 of CH_4 and CO_2 emissions) released as CH_4 were an order of magnitude greater in the young
 622 bog than mature bog stage, at 18 and 2% respectively. This was a result of both higher CH_4
 623 emissions and lower ecosystem respiration (Figure S3) in the young bog. The $\delta^{13}\text{C}-\text{CH}_4$
 624 signature of CH_4 emissions (intercept values from Keeling plots), in the young bog were
 625 significantly greater than those observed in the mature bog (Figure 3c; ANOVA: $F_{(1,4)} =$
 626 $20.67, P < 0.05$). The average $\delta^{13}\text{C}-\text{CH}_4$ signature of CH_4 emissions in the young bog ($n = 4$)
 627 was $-66.5 \pm 1.4\text{‰}$ (95% CI) and $78.5 \pm 5.6\text{‰}$ (95% CI; Figure 3c) in the mature bog
 628 emissions ($n = 4$).



629

630 **Figure 3.** Magnitude and isotopic signature of greenhouse gas fluxes from the young bog
 631 (green) and mature bog (yellow) shown as boxplots. Boxes represents the interquartile range
 632 (25 – 75%), with median shown as black horizontal line. Whiskers extend to 1.5 times the
 633 interquartile range (distance between first and third quartile) in each direction, with outlier

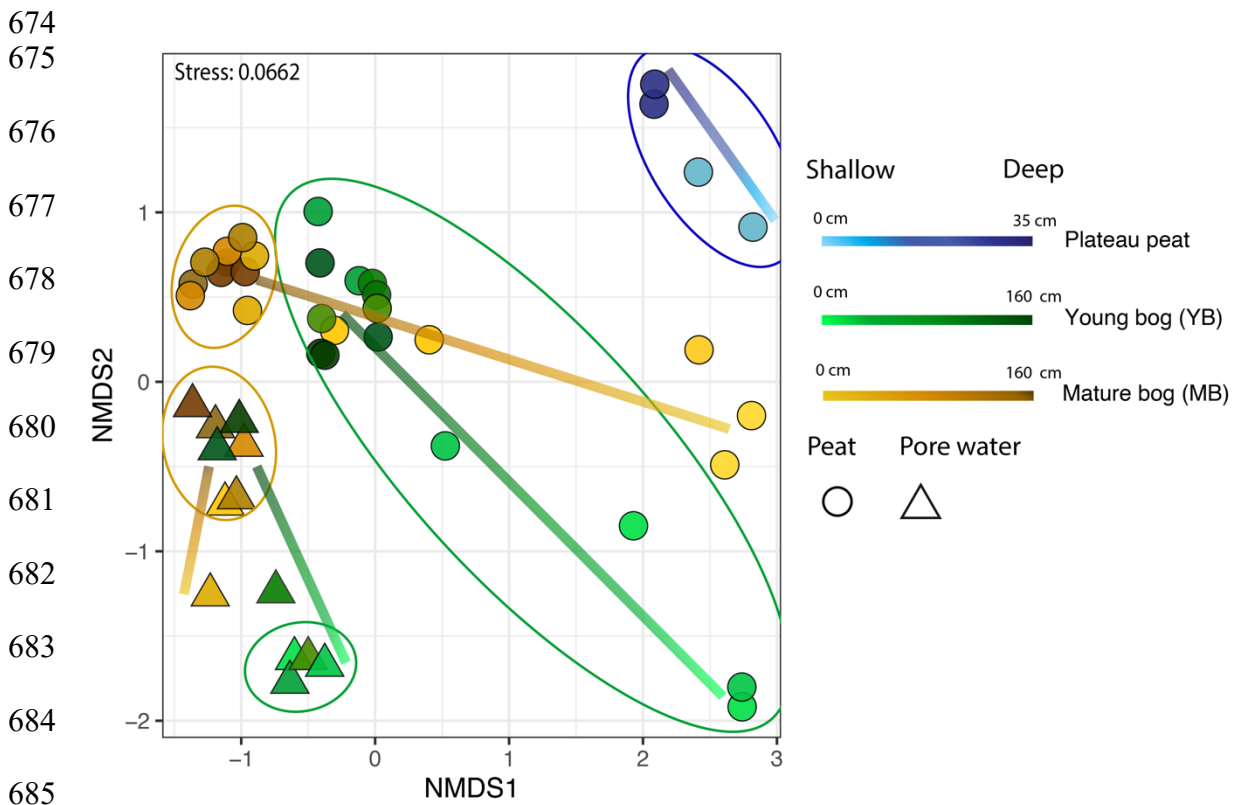
634 data plotted individually as black dots (a) The magnitude of net land-atmosphere CH₄
635 emissions as measured by soil chambers. (b) The ratio between CH₄ emissions and the sum of
636 CO₂ emissions (ecosystem respiration) and CH₄, both standardized to per g C. (c) Intercept
637 values of Keeling plots indicating the $\delta^{13}\text{C-CH}_4$ signature of CH₄ emissions. Isotopically
638 heavier (i.e., less negative) $\delta^{13}\text{C-CH}_4$ is produced via acetoclastic methanogenesis, whereas
639 isotopically lighter (i.e., more negative) $\delta^{13}\text{C-CH}_4$ is produced via hydrogenotrophic
640 methanogenesis. The CH₄ and CO₂ land-atmosphere fluxes shown in (a) and (b) were
641 measured once a month from May – September 2018. The $\delta^{13}\text{C-CH}_4$ of CH₄ emitted to the
642 atmosphere was measured in September and October 2016 (see methods for details and
643 Figure S4 for Keeling plots).

644

645 *3.4 Microbial community structure along the permafrost peatland thaw gradient*

646 We used NMDS ordinations to assess differences in microbial community structure
647 between solid peat and pore water samples, between sampling depths, and between the
648 plateau, young bog, and mature bog. The only exception was the plateau, where only peat
649 samples were collected (i.e., no pore water samples). Microbial community structure in peat
650 was determined to be significantly different from porewater microbial communities
651 (PERMANOVA, $R^2 = 0.13$, $P < 0.05$, Figure 4). The differences observed in the microbial
652 community structure between peat and pore water samples could be a function of the
653 different extraction methods used to extract DNA (Carrigg et al., 2007). Among the pore
654 water samples, distinct microbial communities were found to be associated with the young
655 bog and mature bog. Similarly, microbial community structure in peat was found to be
656 significantly distinct between the three successional stages (plateau peat, young bog and
657 mature bog; Figure 4; PERMANOVA, $R^2 = 0.18$, $P < 0.05$). There is also a common trend in
658 vertical community structuring for all sample matrices according to depth. Changes in overall
659 microbial community composition in both peat and pore water, across a vertical profile (to a
660 maximum depth of 160 cm), illustrate a confluence in microbial community structure with
661 depth in both the young and mature bog (Figure 4). In other words, community structure was
662 most dissimilar at depths closer to the surface (Figure 4, Figure S2; PERMANOVA; $R^2 =$

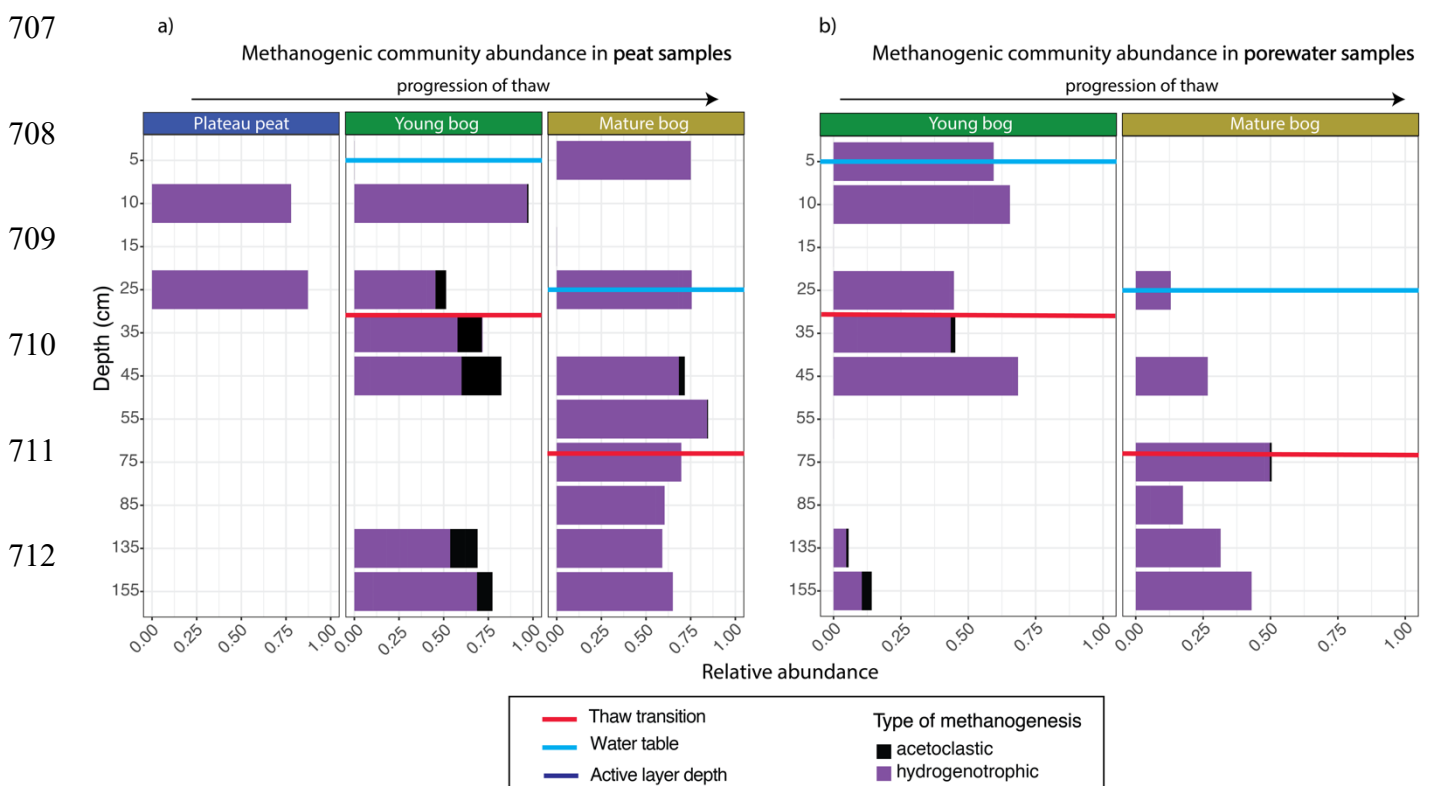
663 0.16, $P < 0.05$). This trend was particularly evident in the porewater samples (Figure 4). In
 664 the peat samples, though microbial communities did not fully converge, deeper young bog
 665 peat (i.e., 90 – 160 cm) communities did become more similar to communities found in the
 666 mature bog at intermediate depths (i.e., 30 – 70 cm), based on the nearness of sample points
 667 on the NMDS (Figure 4). We also observed that the mature bog near-surface peat samples
 668 were located closer to the plateau peat on the NMDS (Figure 4, PERMANOVA, $R^2 = 0.4$, $P =$
 669 0.1). It was not possible to assess the presence of this cyclic succession (from young bog to
 670 mature bog to plateau) in the pore water samples since we did not characterize the microbial
 671 community in the plateau pore water. Finally, we also assessed the effect of seasonality on
 672 microbial community structure and found no effect with regards to sampling month
 673 (PERMANOVA; $R^2 = 0.02$, $P = 0.090$).



686 **Figure 4.** Microbial community distribution according to stage of peat/pore water. NMDS
 687 ordinations of amplicon sequencing variant (ASV) data demonstrate significant community
 688 dissimilarities according to thaw stage for both pore water (shown by the triangles) and peat
 689 (shown by the circles) samples, encircled by 95% confidence intervals. Colour gradient and

690 lines demonstrate the shift in microbial community structure along vertical depth profiles
 691 where lighter shades indicate samples closer to the surface.
 692

693 The total archaeal community comprised 6% of the entire microbial dataset.
 694 Methanogen-related orders comprised 54% of this archaeal dataset and demonstrated marked
 695 differences in the relative abundance of acetoclastic-related methanogens according to thaw
 696 stage and depth in both peat and pore water samples (Figure 5; Figure S2). In the young and
 697 mature bog peat samples, hydrogenotrophic-related methanogens were ubiquitously present
 698 throughout both depth profiles (Figure 5a). In comparison, acetoclastic-related methanogens
 699 exhibited a relatively restricted presence, only present at specific depths (Figure 5a). These
 700 communities were most abundant (>25% of the total methanogenic community) near the
 701 surface in the young bog, just above and below the thaw transition zone (Figure 5a). In the
 702 pore water, hydrogenotrophic methanogens were also dominant throughout depths in both
 703 stages of thaw (Figure 5b). However, in contrast to peat samples, acetoclastic methanogens
 704 were virtually absent in the pore water, although minimally present (i.e., $\leq 10\%$ relative
 705 abundance) at depths between 35 and 155 cm, all found below the thaw transition zone
 706 (Figure 5b).



713

714

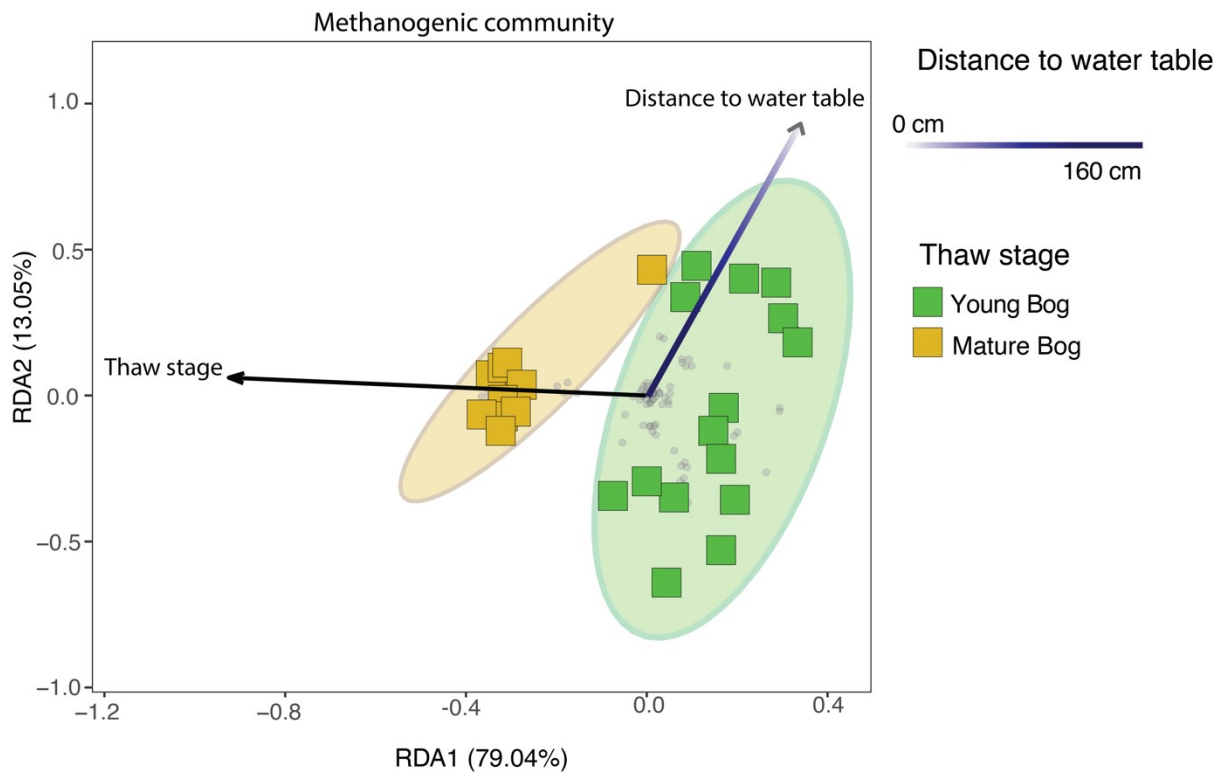
715

716 **Figure 5.** Relative abundance of archaeal orders according to putative methanogenic
717 capability, along a depth profile for peat and pore water samples. Samples are arranged
718 according to depth (y axis), with the relative abundance of methanogenic archaea resolved
719 shown on the x axis. Note that the y axis does not uniformly progress in 10 cm increments.
720 Progression of thaw is shown from plateau peat to young bog to mature bog at the top of the
721 figures, with position of water table shown in blue for each panel. Red lines demonstrate
722 thaw transition zone for the young bog and mature bog. (a) Stacked bar plot of methanogenic
723 Archaea for all peat samples. Samples demonstrate significant differences in putative
724 methanogen composition between all stages (Kruskall-Wallis test & Wilcox rank sum test,
725 with Benjamini-Hochberg corrected p-values, $P < 0.05$). (b) Stacked bar plot of
726 methanogenic Archaea for all pore water samples. Samples do not demonstrate significant
727 differences in putative methanogen composition between stages (Kruskall-Wallis test, with
728 Benjamini-Hochberg corrected p-values, $P = 0.965$).

729

730 Using a redundancy analysis (RDA, Figure 6) we found that 27.6% of variation in the
731 methanogenic community was explained by two variables: thaw stage (ANOVA, $P < 0.05$)
732 and depth from the water table (ANOVA, $P < 0.05$). Although these were the only two
733 parameters that were identified as significant variables impacting microbial community
734 structure when using a backward stepping model, it should be noted that there may be more
735 variation in the community that our experimental design does not take into account as a result
736 of unconstrained variation represented by plant-microbe and/or microbe-microbe interactions
737 (Boon et al., 2014). Nonetheless, the 27.6% variation explained is in accordance with other
738 studies conducted in permafrost impacted regions using similar methods, where the
739 percentage of explained variation falls between 6% (low) to 43% (high) (Comte et al., 2015;
740 Hough et al., 2020). Next, we used variance partitioning to assess the extent to which thaw
741 stage and depth from the water table (i.e., the significant environmental variables identified
742 by the RDA) explained the variation in only the methanogenic community structure (Figure
743 6). Based on this analysis, thaw stage explained 18.4% and distance to the water table
744 explained 4.3% of methanogenic community variation, respectively.

745
746
747
748
749
750
751
752
753
754
755
756
757
758
759
760
761
762
763



764 **Figure 6.** Redundancy analysis (RDA) exploring significant biotic and abiotic variables
765 influencing the total methanogenic community (adjusted $R^2 = 27.6\%$), as determined by a
766 backward stepping RDA model in the peat and pore water samples. All parameters that were
767 used in model are described in section 2.10 of the Methods. Grey dots in the panel
768 demonstrate the distribution of all ASVs in the methanogenic dataset. Shaded ellipses
769 represent the 95% confidence intervals for microbial community structure according to
770 peatland thaw stage (young bog vs mature bog). Only significant (ANOVA, $P < 0.05$)
771 variables are shown. Using variation partitioning, we found that peatland thaw stage
772 significantly explains about 18.4% of methanogenic community variation whereas distance to
773 water table explained 4.3%. Both axes are significant (ANOVA, $P < 0.05$).
774

775 4. Discussion

776 Our study shows that high CH_4 emissions from thermokarst bogs in the initial decades
777 following permafrost thaw (young bog) are not only linked to environmental conditions
778 (wetness, soil temperature, vegetation), but also driven by relatively increased microbial CH_4

779 production through the energetically more favourable acetoclastic methanogenesis pathway.
780 Evidence of putatively acetoclastic methanogens and CH₄ produced via the acetoclastic
781 metabolic pathway was found in the young bog both near the surface and at depths below the
782 thaw transition (i.e., in peat that accumulated prior to permafrost thaw). We are unable to
783 determine whether these greater CH₄ emissions in the initial decades following thaw are due
784 to the mineralization of labile organic matter released from previously frozen peat, or are
785 driven solely by fresh, labile DOM derived from surface vegetation leached throughout the
786 peat profile. However, previous work in the discontinuous permafrost region in the Interior
787 Plains of western Canada has found a limited contribution of previously frozen organic
788 matter contributing to surface CH₄ emissions in thermokarst bogs (Cooper et al., 2017).
789 Elevated CH₄ emissions then slow over the following centuries with succession into a mature
790 thermokarst bog stage where CH₄ production is almost exclusively through the
791 hydrogenotrophic pathway.

792 *4.1 Shift in microbial community assemblages along a permafrost thaw gradient*

793 Microbial communities varied along the permafrost thaw gradient; among different thaw
794 stages (permafrost peat plateau, young bog, and mature bog), with peat depth (surface down
795 to 160 cm), and between different sample types (solid peat and pore water). We found clear
796 differences in microbial communities between the young bog and mature bog, despite similar
797 peat stratigraphy up to the surficial vegetation (Heffernan et al., 2020), where dominant
798 *Sphagnum* species varied. The greater height of the peat surface above the water table and
799 drier conditions in the mature bog, due to the slow accumulation of new peat over centuries,
800 leads to a shift in vegetation composition from hydrophilic *Sphagnum* and graminoids
801 towards more drought resistant *Sphagnum* spp. and ericaceous shrubs. This shift in water
802 table position and vegetation community, along with a decrease in temperatures (Figure S1a)

803 due to the thermal insulating properties of *Sphagnum* peat (Kujala, Seppälä, & Holappa,
804 2008) appears to have caused the observed differences in microbial communities between the
805 young and mature bog, even at depths >1 m. Microbial communities were most dissimilar
806 between the peat plateau and young bog. This was unsurprising given the abrupt shift from
807 the elevated, frozen, and relatively dry peat plateau forest to the young bog where the surface
808 was saturated, dominated by hydrophilic vegetation and had warmer temperatures. We
809 further noted that the microbial community of the mature bog was more similar with the peat
810 plateau than with the young bog. Paleo-records in the region (Heffernan et al., 2020; Pelletier
811 et al., 2017; Zoltai, 1993) show that many peatlands have undergone cyclical permafrost
812 developments, as thermal insulating properties of *Sphagnum* peat in mature bogs leads to the
813 re-aggradation of permafrost peat plateaus. Our study suggests that the peat plateau microbial
814 community is influenced by the preceding mature bog microbial community as permafrost
815 aggrades.

816 The most dissimilar microbial community composition was observed between
817 samples near the surface and those at depth (i.e., down to 160 cm), as has also been
818 observed in other permafrost ecosystems (Frey et al., 2016; Monteux et al., 2018). Shifts in
819 microbial community composition along the thaw gradient were most evident nearer the
820 surface, whereas communities found at depth were similar between the young bog and mature
821 bog (Figure 4). At the surface, microbial community structure is influenced by the
822 successional vegetation community (Hodgkins et al., 2014) and the role that vegetation,
823 particularly graminoids which are found in the young bog, has on microbial community
824 structure has been well documented in northern peatlands (Robroek et al., 2015, 2021;
825 Bragazza et al., 2015). Moderately acidic, saturated peatlands with hydrophilic vegetation,
826 similar to the young bog, have been shown to harbour acid tolerant fermenting bacteria that
827 produce substrates for methanogenesis and are trophically linked with methanogens (Wüst et

828 al., 2009). Thus, the interaction between water table position, pH, and vegetation community
829 influences the substrates available to the microbial community, which in turn impacts the
830 surface community's structure (Kotiaho et al., 2013). In contrast, communities at depth are
831 known to be influenced by peat properties, such as peat chemistry and degree of
832 decomposition, and the paleoenvironment under which they originally colonized (Lee et al.,
833 2012; Holm et al., 2020). In the young and mature bog both peat properties (humification
834 indices including FTIR 1630/1090 cm^{-3} and C:N ratios) and the paleoenvironment at depth
835 are similar (Heffernan et al., 2020), which may explain the observed convergence of
836 microbial community structure. Nonetheless, although there are some similarities at depth
837 between both young and mature bog, microbial communities inhabiting either are still distinct
838 (Figure 4). This is emphasized by the differing abundance of Archaea that participate in
839 hydrogenotrophic or acetoclastic methanogenesis (Figure 5) in both stages down the peat
840 profile.

841 As has been shown previously in other thermokarst peatlands (McCalley et al., 2014),
842 the young and mature bog stages were dominated by hydrogenotrophic methanogens.
843 However, putatively acetoclastic methanogens were relatively more abundant in the young
844 bog (Figure 5), particularly at or below the transition in peat that accumulated prior to
845 permafrost thaw. Thaw stage and distance from the water table were found to influence the
846 methanogenic community composition (Figure 6), with distance from the water table
847 dictating where anoxic conditions persist (Blodau et al., 2004) and thus where methanogenic
848 colonization can occur. The influence of vegetation communities associated with different
849 thermokarst peatland stages on methanogenic community composition has previously been
850 attributed to the role of plant derived DOM serving as the substrate for CH_4 production
851 (Liebner et al., 2015; McCalley et al., 2014). The presence of hydrophilic vegetation,
852 particularly graminoids, in the saturated young bog provides the precursors for fermentation,

853 yielding acetate (Liebner et al., 2015; Ström et al., 2003, 2012, 2015) and serving as the
854 substrate for acetoclastic CH₄ production. The downward transport from the surface of plant
855 derived DOM in the young bog (Chanton et al., 2008) likely provides sufficient acetate for
856 the establishment of acetoclastic methanogens at depth in this environment.

857 *4.2 . Production and emissions of CH₄ along a peatland thaw gradient*

858 Isotopic signatures ($\delta^{13}\text{C}$) of dissolved CO₂ and CH₄ and α_{C} values in porewater and
859 the of $\delta^{13}\text{C}$ signature of CH₄ emitted to the atmosphere provided further evidence of
860 relatively elevated acetoclastic methanogenesis in the young bog stage. The general increase
861 in $\delta^{13}\text{C}$ -CO₂ with depth observed at both sites (Figure 2d) indicates accumulation of
862 isotopically heavier $\delta^{13}\text{C}$ -CO₂ which is likely explained by the preferential use of isotopically
863 lighter $\delta^{13}\text{C}$ -CO₂ during hydrogenotrophic methanogenesis (Hornibrook et al., 2000). As a
864 result, CH₄ tends to become lighter with depth and this was particularly apparent in the
865 mature bog (Figure 2c). This leads to the average α_{C} values of 1.064 ($\delta^{13}\text{C}$ -CH₄; -68.7‰) in
866 the mature bog, which were significantly higher than the 1.058 ($\delta^{13}\text{C}$ -CH₄; -62.4‰) observed
867 in the young. Together, the $\delta^{13}\text{C}$ -CH₄ and $\delta^{13}\text{C}$ -CO₂ data and the resulting α_{C} depth profiles
868 suggest that the majority of CH₄ is produced via the hydrogenotrophic methanogenic
869 pathway, which supports the findings of the microbial community analysis (Figure 5). Our
870 isotope data also suggests that a greater proportion of CH₄ is produced via acetoclastic
871 methanogenesis throughout the profile in the young bog compared to the mature bog (Figure
872 2c – f). This is evident from lower average α_{C} values found in the young bog compared to the
873 mature bog, and greater number of these young bog α_{C} values falling between 1.040 – 1.065
874 which represents acetoclastic methanogenesis (Whiticar, 1999). These findings again agree
875 with the relatively greater abundance of acetoclastic methanogens observed at that site
876 (Figure 5).

877 In this study we found that average CH₄ emissions in the initial decades following thaw,
878 in the young bog stage, were 2.5 – 3 times greater than emissions measured in the mature bog
879 stage which had thawed ~200 years ago (Figure 3a). Furthermore, the proportion of CH₄ to
880 overall C emissions (Figure 3b) was considerably greater in the young bog than in the mature
881 bog. In the mature bog the lower water table position leads to both increased CO₂ emissions
882 and decreased CH₄ emissions, resulting in a reduced fraction of C emissions as CH₄. Previous
883 studies have shown similarly increased CH₄ emissions in the initial decades following thaw
884 (Johnston et al., 2014; Wickland et al., 2006). While our pore water chemistry data is
885 inconclusive with regards to organic carbon characteristics, other work in thermokarst bogs in
886 the Interior Plains of western Canada has shown that the organic matter derived from the
887 young bog vegetation community is highly labile (Burd et al., 2020). Previous work at our
888 study site has shown that the vegetation community in the young bog is associated with
889 greater potential enzymatic degradation of organic matter (Heffernan et al., 2021). Hydrolysis
890 of plant derived organic matter by extracellular enzymes leads to the formation of monomers
891 (Kotsyurbenko, 2005). These monomers can be further degraded to form acetate and other
892 precursors for methanogenesis when present with anaerobic fermenting bacteria (Hamberger
893 et al., 2008) and near the surface and vegetation inputs (Hädrich et al., 2012). Our study
894 shows that these higher CH₄ emissions are likely linked to increased wetness, temperatures,
895 and a vegetation community associated with more labile organic matter which favour a
896 greater proportion of CH₄ produced via acetoclastic methanogenesis, as shown by our $\delta^{13}\text{C}$ -
897 CH₄, α_c depth profiles and microbial community composition analyses.

898 Many factors, including environmental conditions and microbial community structure
899 likely contribute to the differences in net CH₄ emissions from the young and mature bog
900 (Figure 3a). Methane oxidation has been shown to be an important regulator of post-thaw
901 CH₄ emissions (Perryman et al., 2020) and to result in isotopically heavier (i.e., less negative)

902 $\delta^{13}\text{C}\text{-CH}_4$ and lighter (i.e., more negative) $\delta^{13}\text{C}\text{-CO}_2$ (Whiticar, 1999). Our data suggests the
903 role of CH_4 oxidation was different between sites. Methane oxidation was apparent in the
904 $\delta^{13}\text{C}\text{-CH}_4$ and $\delta^{13}\text{C}\text{-CO}_2$ signatures above the water table in the mature bog but no CH_4
905 oxidation is evident in the young bog (Figure 2c, d). The difference in gas flux $\delta^{13}\text{C}$
906 signatures (Figure 3c) also suggests a greater prevalence of CH_4 oxidation in the mature bog.
907 However, increased oxidation above the water table in the mature bog is likely not fully
908 responsible for the observed differences in CH_4 surface emissions and depth profiles between
909 the young and mature bog. Lower soil temperatures, a vegetation community associated with
910 reduced substrate availability, the dominance of hydrogenotrophic methanogenesis
911 throughout the peat profile, and a deeper water table position all contribute to the lower CH_4
912 production and higher CH_4 oxidation observed in the mature bog. Nonetheless, using this
913 interdisciplinary approach, we are unable to determine the relative contribution of
914 acetoclastic methanogenesis at each depth to the overall emissions at the surface.

915 Our results, and those of others (Euskirchen et al., 2014; Johnston et al., 2014), have
916 shown that CH_4 emissions exhibit seasonal variation (Figure S3a, c). However, in contrast to
917 some previous findings (Ebrahimi & Or, 2017), we did not observe a corresponding seasonal
918 response in the microbial community composition (Figure S2). This may be a sampling
919 design effect since our study spanned only two months (June and September), compounded
920 by the fact that we did not have replicate samples to test the robustness of this finding.
921 However, other studies have also shown that soil microbial community growth is not
922 impacted by seasonal variations in temperature (Simon et al., 2020) and that microbial
923 communities require a longer time scale (years-decades-centuries) to respond to temperature
924 following thaw (Feng et al., 2020). Our results corroborate these observations, suggesting a
925 long-term response in the microbial community composition to the ecological shifts
926 associated with autogenic peatland succession following permafrost thaw. Autogenic

927 peatland succession following thaw occurs on the decade to century timescale, shifting from
928 recently thawed to mature thermokarst bogs (Camill, 1999). Both recently thawed (young)
929 and mature thermokarst bogs have distinct hydrological regimes, vegetation communities,
930 and peat chemistry. Following thaw, associated changes in vegetation and litter input alters
931 microbial community composition and activity (Adamczyk et al., 2020; Kirkwood et al.,
932 2021). Such changes in microbial community structure thus impact CH₄ emissions from
933 thermokarst peatlands. Under predicted climatic warming scenarios differences in microbial
934 community composition have been shown to be increasingly driven by seasonally
935 independent variables such as substrate quality and the legacy effects of soil temperatures
936 (Luláková et al., 2019). This study suggests that the environmental conditions required for
937 increased methanogenic activity at depth is limited to the initial decades following thaw, after
938 which the microbial community structure changes in response to lowering of the water table,
939 lower soil temperatures and shifts in the vegetation community.

940 **5. Conclusion**

941 This study demonstrates that higher CH₄ emissions in thermokarst bogs in the initial
942 decades following thaw are driven by shifts in vegetation communities that produce organic
943 matter inputs of varying lability (Burd et al., 2020) and prevalence of anoxic conditions,
944 which was associated with an increase of acetoclastic methanogenesis in our site. The
945 influence of this pathway was apparent at depth throughout the peat profile. With succession
946 following thaw towards a mature thermokarst bog, a shift in water table position and
947 vegetation composition seems to reduce the role of acetoclastic methanogenesis pathway.
948 Previous work at this site (Heffernan et al., 2021) and other thermokarst peatlands in the
949 discontinuous permafrost zone of boreal western Canada (Burd et al., 2020) have indicated
950 that the vegetation community found in the initial decades following permafrost thaw is

951 associated with increased potential enzymatic degradation and biodegradability of organic
952 matter compared to that found in the mature bog. Average growing season CH₄ emissions
953 were 2.5 – 3 times greater in the recently thawed young bog. Overall, C emissions in the
954 young bog contained proportionally more CH₄ than those from the mature bog, due to greater
955 CH₄ production and also reduced CO₂ emissions. These greater CH₄ emissions in the young
956 bog are driven by a higher contribution to surface emissions from CH₄ produced throughout
957 the peat profile by acetoclastic methanogens. The response of the microbial community to
958 permafrost thaw is tied to the shifting environmental conditions associated with peatland
959 autogenic succession. Warmer and wetter conditions in the initial decades following thaw, in
960 conjunction with a vegetation community associated with greater availability of labile plant
961 leachates (Bragazza et al., 2015), provides favourable conditions for acetoclastic
962 methanogens throughout the peat profile. Given the projected increases in thermokarst
963 peatland formation (Olefeldt et al., 2016), our study suggests that we can expect a pulse of
964 CH₄ emissions from current regions of the discontinuous permafrost zone. This pulse will be
965 driven, in part, by increased acetoclastic methanogenesis from labile substrates in recently
966 thawed thermokarst peatlands. However, this rapid increase in CH₄ emissions will only
967 remain at the decadal to century scale as autogenic peatland succession results in relatively
968 drier mature thermokarst bogs, where lower temperatures and less labile substrate availability
969 leads to a dominance of hydrogenotrophic methanogenesis.

970

971 **Data availability**

972 All biogeochemical and enzyme datasets generated and analyzed during this study are
973 available in the UAL Dataverse repository, [<https://doi.org/10.5683/SP3/5TSH9V>]. Microbial
974 sequences used in this study can be accessed from the NCBI database, using accession
975 number PRJNA660023.

976

977 **Author contributions**

978 All authors contributed to the conception of the work. LH and CEA performed the field work
979 component. LH performed the biogeochemistry measurements. MAC performed the
980 microbial measurements. LH and MAC analyzed the data and wrote the manuscript draft. All
981 authors reviewed and edited the manuscript.

982 **Competing interests**

983 The authors declare that they have no conflict of interest.

984 **Acknowledgements**

985 The authors wish to thank McKenzie Kuhn, Maya Frederickson, Jördis Stührenberg, and
986 Trisha Elliot for assistance with field and lab work. We also thank Sophie Dang, at MBSU
987 for providing guidance throughout 16S rRNA gene library building and for subsequently
988 sequencing these libraries at the MBSU facility.

989 **Financial support**

990 Funding and support were provided to D. Olefeldt and M. Bhatia by the Natural Science and
991 Engineering Research Council of Canada, Discovery grant (RGPIN-2016-04688 to DO and
992 RGPIN-2020-05975 to MB) and the Campus Alberta Innovates Program (CAIP).

993

994

995

996 **References**

997 Adamczyk, M., Perez-Mon, C., Gunz, S., Frey, B. (2020). Strong shifts in microbial
998 community structure are associated with increased litter input rather than temperature in High
999 Arctic soils. *Soil Biology and Biochemistry* 151: 1-14.
1000 <https://doi.org/10.1016/j.soilbio.2020.108054>
1001
1002 Allan, E., Manning, P., Alt, F., Binkenstein, J., Blaser, S., Blüthgen, N., et al.
1003 (2015). Land use intensification alters ecosystem multifunctionality via loss of biodiversity
1004 and changes to functional composition. *Ecology Letters* 18: 834–843
1005 <https://doi.org/10.1111/ele.12469>
1006
1007 Baltzer J.L., Veness T., Chasmer L.E., Sniderhan, A.E., Quinton, W.L. (2014). Forests on
1008 thawing permafrost: fragmentation, edge effects, and net forest loss. *Global Change Biology*
1009 20: 824–834. doi: 10.1111/gcb.12349
1010
1011 Bauer, I. E., Gignac, L. D., Vitt, D. H. (2003). Development of a peatland complex in boreal
1012 western Canada: Lateral site expansion and local variability in vegetation succession and
1013 long-term peat accumulation. *Canadian Journal of Botany* 81: 833–847.
1014 <https://doi.org/10.1139/b03-076>
1015
1016 Beilman, D. W. (2001). Plant community and diversity change due to localized permafrost
1017 dynamics in bogs of western Canada. *Canadian Journal of Botany* 79: 983–993.
1018 <https://doi.org/10.1139/cjb-79-8-983>
1019
1020 Bellisario, L. M., Bubier, J. L., Moore, T. R., Chanton, J. P. (1999). Controls on CH₄
1021 emissions from a northern peatland. *Global Biogeochemical Cycles*, 13: 81-91
1022 [..https://doi.org/10.1029/1998GB900021](https://doi.org/10.1029/1998GB900021)
1023
1024 Berghuis, B.A., Yu, F.B., Schulz, F., Blainey, P.C., Woyke, T., Quake, S.R. (2019).
1025 Hydrogenotrophic methanogenesis in archaeal phylum Verstraetearchaeota reveals the shared
1026 ancestry of all methanogens. *PNAS* 116 (11): 5037-5044.
1027 <https://doi.org/10.1073/pnas.1815631116>
1028
1029 Blodau, C., Basiliko, N., Moore, T. R. (2004). Carbon turnover in peatland mesocosms
1030 exposed to different water table levels. *Biogeochemistry* 67: 331-351
1031 https://doi.org/10.1023/B:BIOG.0000015788.30164.e_2
1032
1033 Boon, E., Meehan, C. J., Whidden, C., Wong, D. H., Langille, M. G., Beiko, R. G. (2014).
1034 Interactions in the microbiome: communities of organisms and communities of genes. *FEMS*
1035 microbiology reviews 38: 90–118. <https://doi.org/10.1111/1574-6976.12035>
1036
1037 Bragazza, L., Bardgett, R. D., Mitchell, E. A. D., Buttler, A. (2015). Linking soil microbial
1038 communities to vascular plant abundance along a climate gradient. *New Phytologist* 205:
1039 1175–1182. <https://doi.org/10.1111/nph.13116>
1040

1041 Bridgham, S. D., Cadillo-Quiroz, H., Keller, J. K., Zhuang, Q. (2013). Methane emissions
1042 from wetlands: Biogeochemical, microbial, and modeling perspectives from local to global
1043 scales. *Global Change Biology* 19: 1325-1346 <https://doi.org/10.1111/gcb.12131>
1044

1045 Brown, J., Ferrians Jr., O. J., Heginbottom, J. A., Melnikov, E. S. (1997). Circum-Arctic map
1046 of permafrost and ground ice conditions. USGS Numbered Series, 1.
1047 <https://doi.org/10.1016/j.jallcom.2010.03.054>
1048

1049 Burd, K., Estop-Aragónés, C., Tank, S. E., Olefeldt, D. (2020). Lability of dissolved
1050 organic carbon from boreal peatlands: interactions between permafrost thaw, wildfire,
1051 and season. *Canadian Journal of Soil Science* 13: 1–13.
1052 <https://doi.org/10.1139/cjss-2019-0154>
1053

1054 Burger, M., Berger, S., Spangenberg, I., Blodau, C. (2016). Summer fluxes of methane and
1055 carbon dioxide from a pond and floating mat in a continental Canadian peatland.
1056 *Biogeosciences*. 13: 3777-3791. <https://doi.org/10.5194/bg-13-3777-2016>.
1057

1058 Cai, L., Alexeev, V.A., Arp, C.D., Jones, B.M., Liljedahl, A., Gadeke, A. (2016). Dynamical
1059 Downscaling data for studying climactic impacts on hydrology, permafrost and ecosystem in
1060 Arctic Alaska. *Earth System Science Data Discussion* [preprint] 1-38. doi:10.5194/tc-2016-
1061 87
1062

1063 Camill, P. (1999). Peat accumulation and succession following permafrost thaw in the Boreal
1064 peatlands of Manitoba, Canada. *Ecoscience* 6: 592–602.
1065 <https://doi.org/10.1080/11956860.1999.11682561>
1066

1067 Carrigg, C., Rice, O., Kavanagh, S., Collins, G., O’Flaherty, V. (2007). DNA extraction
1068 method affects microbial community profiles from soils and sediment. *Applied Microbiology*
1069 *and Biotechnology* 77: 955-964.
1070

1071 Carroll, P., Crill, P. (1997). Carbon balance of a temperate poor fen. *Global*
1072 *Biogeochemical Cycles*. <https://doi.org/10.1029/97GB01365>
1073

1074 Carson, M.A, Bräuer, S., Basiliko, N. (2019). Enrichment of peat yields novel methanogens:
1075 approaches for obtaining uncultured organisms in the age of rapid sequencing, *FEMS*
1076 *Microbiology Ecology* 95:1-11. <https://doi.org/10.1093/femsec/fiz001>
1077

1078 Chanton, J., Chaser, L., Glasser, P., Siegel, D. (2005). Carbon and Hydrogen Isotopic
1079 Effects in Microbial, Methane from Terrestrial Environments. *Stable Isotopes and*
1080 *Biosphere - Atmosphere Interactions*, Elsevier Inc. 85–105. <https://doi.org/10.1016/B978-012088447-6/50006-4>
1081 012088447-
1082 6/50006-4
1083

1084 Chanton, J. P., Glaser, P. H., Chasar, L. S., Burdige, D. J., Hines, M. E., Siegel, D. I., ...

1085 Cooper, W. T. (2008). Radiocarbon evidence for the importance of surface vegetation on
1086 fermentation and methanogenesis in contrasting types of boreal peatlands. *Global*
1087 *Biogeochemical Cycles*, 22(4), 1–11. <https://doi.org/10.1029/2008GB003274>
1088 Climate-Data.org. (2019). Retrieved January 21, 2019, from 2019 website:
1089 <https://en.climate-data.org/north-america/canada/alberta/meander-river-11380/>
1090
1091 Chasar, L. S., Chanton, J. P., Glaser, P. H., Siegel, D. I., and Rivers, J. S. (2000),
1092 Radiocarbon and stable carbon isotopic evidence for transport and transformation of
1093 dissolved organic carbon, dissolved inorganic carbon, and CH₄ in a northern Minnesota
1094 peatland, *Global Biogeochemical Cycles*: 14, 1095–1108, doi:10.1029/1999GB001221.
1095
1096 Chasmer, L. and Hopkinson, C. (2017), Threshold loss of discontinuous permafrost and
1097 landscape evolution. *Glob Change Biology* 23: 2672-2686. <https://doi.org/10.1111/gcb.13537>
1098
1099 Cooper, M. D. A., Estop-Aragonés, C., Fisher, J. P., Thierry, A., Garnett, M. H., Charman, D.
1100 J et al.,(2017). Limited contribution of permafrost carbon to methane release from thawing
1101 peatlands. *Nature Climate Change* 7: 507–511. <https://doi.org/10.1038/nclimate3328>
1102
1103 Comte, J., Monier, A., Crevecoeur, S., Lovejoy, C., Vincent, W.F.(2015). Microbial
1104 biogeography of permafrost thaw ponds across the changing northern landscape. *Ecography*
1105 39: 609-618.
1106
1107 Connon, R.F., Quinton, W.L., Craig, J.R., Hayashi, M. (2014). Changing hydrologic
1108 connectivity due to permafrost thaw in the lower Liard River valley, NWT, Canada.
1109 *Hydrological Processes* 28: 4163-4178. <https://doi.org/10.1002/hyp.10206>
1110
1111 Conrad, R. (1999). Contribution of hydrogen to methane production and control of hydrogen
1112 concentrations in methanogenic soils and sediments. *FEMS Microbiology Ecology* 28: 193-
1113 202
1114 [https://doi.org/10.1016/S0168-6496\(98\)00086-5](https://doi.org/10.1016/S0168-6496(98)00086-5)
1115
1116 Corbett, J. E., Tfaily, M. M., Burdige, D. J., Cooper, W. T., Glaser, P. H., Chanton, J. P.
1117 (2013). Partitioning pathways of CO₂ production in peatlands with stable carbon
1118 isotopes. *Biogeochemistry*, 114: 327-340. <https://doi.org/10.1007/s10533-012-9813-1>
1119
1120 Criquet, S., Farnet, A. M., Tagger, S., Le Petit, J. (2000). Annual variations of
1121 phenoloxidase activities in an evergreen oak litter: Influence of certain biotic and abiotic
1122 factors. *Soil Biology and Biochemistry* 32: 1505-1513. [https://doi.org/10.1016/S0038-](https://doi.org/10.1016/S0038-0717(00)00027-4)
1123 [0717\(00\)00027-4](https://doi.org/10.1016/S0038-0717(00)00027-4)
1124
1125 Dunn, C., Jones, T.G, Girard, A., Freeman, C. (2014). Methodologies for Extracellular
1126 enzyme assays from wetland soils. *Wetlands* 34: 9-17. [https://doi.org/10.1007/s13157-013-](https://doi.org/10.1007/s13157-013-0475-0)
1127 [0475-0](https://doi.org/10.1007/s13157-013-0475-0).
1128

1129 Ebrahimi, A., Or, D. (2017). Mechanistic modeling of microbial interactions at pore to profile
1130 scale resolve methane emission dynamics from permafrost soil. *Journal of*
1131 *Geophysical Research: Biogeosciences* 122: 1216-1238.
1132 <https://doi.org/10.1002/2016JG003674>
1133
1134
1135 Euskirchen, E. S., Edgar, C. W., Turetsky, M. R., Waldrop, M. P., Harden, J. W. (2014).
1136 Differential response of carbon fluxes to climate in three peatland ecosystems that vary in the
1137 presence and stability of permafrost. *Journal of Geophysical Research:*
1138 *Biogeosciences* 119: 1576-1595. <https://doi.org/10.1002/2014JG002683>
1139
1140 Feng, J., Wang, C., Lei, J., Yang, Y., Yan, Q., Zhou, et al. (2020). Warming-induced
1141 permafrost thaw exacerbates tundra soil carbon decomposition mediated by microbial
1142 community. *Microbiome* 8: 1-12. <https://doi.org/10.1186/s40168-019-0778-3>
1143
1144 Fisher, R. E., France, J. L., Lowry, D., Lanoisellé, M., Brownlow, R., Pyle, J. A., et al.
1145 (2017). Measurement of the ¹³C isotopic signature of methane emissions from northern
1146 European wetlands. *Global Biogeochemical Cycles* 31: 605-
1147 623. <https://doi.org/10.1002/2016GB005504>
1148
1149 Fox, J., Weisberg, S. (2011). *An R Companion to Applied Regression*, second ed.
1150 <https://doi.org/10.1016/j.stomax.2010.07.001>
1151
1152 Frey, B., Rime, T., Phillips, M., Stierli, B., Hajdas, I., Widmer, F., Hartmann, M. (2016).
1153 Microbial diversity in European alpine permafrost and active layers. *FEMS microbiology*
1154 *Ecology* 92:1-16. doi.org/10.1093/femsec/fiw018
1155
1156 Fritze, H., Penttilä, T., Mäkiranta, P., Laiho, R., Tuomivirta, T., Forsman, J., et al. (2021).
1157 Exploring the mechanisms by which reindeer droppings induce fen peat methane production.
1158 *Soil Biology and Biochemistry* 160:1-7. <https://doi.org/10.1016/j.soilbio.2021.108318>
1159
1160 Galand, P. E., Fritze, H., Conrad, R., Yrjälä, K. (2005). Pathways for methanogenesis and
1161 diversity of methanogenic archaea in three boreal peatland ecosystems. *Applied and*
1162 *Environmental Microbiology* 71: 2195–2198. [https://doi.org/10.1128/AEM.71.4.2195-](https://doi.org/10.1128/AEM.71.4.2195-2198.2005)
1163 [2198.2005](https://doi.org/10.1128/AEM.71.4.2195-2198.2005)
1164
1165 Gibson, C. M., Chasmer, L. E., Thompson, D. K., Quinton, W. L., Flannigan, M. D.,
1166 Olefeldt, D. (2018). Wildfire as a major driver of recent permafrost thaw in boreal
1167 peatlands. *Nature Communications*, 9: .1-9. <https://doi.org/10.1038/s41467-018-05457-1>
1168
1169 Grant, R. F. (2015). Ecosystem CO₂ and CH₄ exchange in a mixed tundra and a fen within a
1170 hydrologically diverse Arctic landscape: 2. Modeled impacts of climate change. *Journal of*
1171 *Geophysical Research: Biogeosciences*, 120: 1388-1406.
1172 <https://doi.org/10.1002/2014JG002889>

1173

1174 Hädrich, A., Heuer, V.B., Herrmann, M., Hinrichs, K.W., Küsel, K. (2012). Origin and fate of
 1175 acetate in an acidic fen, FEMS Microbiology Ecology 81: 339–354.
 1176 <https://doi.org/10.1111/j.1574-6941.2012.01352.x>
 1177

1178 Hamberger, A., Horn, M.A., Dumont, M.G., Murrell, J.C., Drake H.L. (2008). Anaerobic
 1179 consumers of monosaccharides in a moderately acidic fen. *Applied Environmental*
 1180 *Microbiology* 74: 3112–3120. <https://doi.org/10.1128/AEM.00193-08>
 1181

1182 Hansen, A. M., Kraus, T. E. C., Pellerin, B. A., Fleck, J. A., Downing, B. D., Bergamaschi,
 1183 B. A. (2016). Optical properties of dissolved organic matter (DOM): Effects of biological and
 1184 photolytic degradation. *Limnology and Oceanography* 61: 1015-1032.
 1185 <https://doi.org/10.1002/lno.10270>
 1186

1187 Heffernan, L., Estop-Aragónés, C., Knorr, K.-H., Talbot, J., Olefeldt, D. (2020). Long-term
 1188 impacts of permafrost thaw on carbon storage in peatlands: deep losses offset by
 1189 surficial accumulation. *Journal of Geophysical Research: Biogeosciences* 125:
 1190 e2019JG005501. <https://doi.org/10.1029/2019JG005501>
 1191

1192 Heffernan, L., Jasey, V.E.J., Frederickson, M., Mackenzie, M.D., Olefeldt, D. (2021).
 1193 Constraints on potential enzyme activities in thermokarst bogs: Implications for the carbon
 1194 balance of peatlands following thaw. *Global Change Biology*, 27: 4711-4726.
 1195 <https://doi.org/10.1111/gcb.15758>
 1196

1197 Heginbottom, J. A., Dubreuil, M. H., Harker, P. T. (1995). Canada, Permafrost. National
 1198 Atlas of Canada.
 1199

1200 Helbig, M., Pappas, C., Sonnentag, O. (2016). Permafrost thaw and wildfire: Equally
 1201 important drivers of boreal tree cover changes in the Taiga Plains, Canada. *Geophysical*
 1202 *Research Letters* 43: 1598-1606. <https://doi.org/10.1002/2015GL067193>
 1203

1204 Helms, J.R., Stubbins, A., Ritchie, J.D., Minor, E.C., Kieber, D.J., Mopper, K. (2008).
 1205 Absorption spectral slopes and slope ratios as indicators of molecular weight, source, and
 1206 photobleaching of chromophoric dissolved organic matter. *Limnology and Oceanography*,
 1207 53: 955-969. <https://doi.org/10.4319/lo.2008.53.3.0955>
 1208

1209 Hodgkins, S. B., Tfaily, M. M., McCalley, C. K., Logan, T. A., Crill, P. M., Saleska, S. R. et
 1210 al. (2014). Changes in peat chemistry associated with permafrost thaw
 1211 increase greenhouse gas production. *Proceedings of the National Academy of Sciences*
 1212 111: 5819–5824. <https://doi.org/10.1073/pnas.1314641111>
 1213

1214 Hoffman, G.E., Schadt, E.E. (2016). variancePartition: interpreting drivers of variance in
 1215 complex gene expression studies. *BMC bioinformatics* 17: 1-13.
 1216 <https://doi.org/10.1186/s12859-016-1323-z>

1217
1218 Holm, S., Walz, J., Horn, F., Yang, S., Grigoriev, M. N., Wagner, D., et al. (2020).
1219 Methanogenic response to long-term permafrost thaw is determined by paleoenvironment.
1220 FEMS Microbiology Ecology 96: 1-13.. <https://doi.org/10.1093/femsec/fiaa021>
1221
1222 Hopple, A. M., Wilson, R. M., Kolton, M., Zalman, C. A., Chanton, J. P., Kostka, J., et al.
1223 (2020). Massive peatland carbon banks vulnerable to rising
1224 temperatures. Nature Communications 11: 1-7 [https://doi.org/10.1038/s41467-020-](https://doi.org/10.1038/s41467-020-16311-8)
1225 [16311-8](https://doi.org/10.1038/s41467-020-16311-8)
1226
1227 Hornibrook, E. R. C., Longstaffe, F. J., Fyfe, W. S. (1997). Spatial distribution of
1228 microbial methane production pathways in temperate zone wetland soils: Stable carbon
1229 and hydrogen isotope evidence. Geochimica et Cosmochimica Acta 61: 745–753.
1230 [https://doi.org/https://doi.org/10.1016/S0016-7037\(96\)00368-7](https://doi.org/10.1016/S0016-7037(96)00368-7)
1231
1232 Hornibrook, E. R. C., Longstaffe, F. J., Fyfe, W. S. (2000). Evolution of stable carbon
1233 isotope compositions for methane and carbon dioxide in freshwater wetlands and other
1234 anaerobic environments. Geochimica et Cosmochimica Acta 64: 1013-1027.
1235 [https://doi.org/10.1016/S0016-7037\(99\)00321-X](https://doi.org/10.1016/S0016-7037(99)00321-X)
1236
1237 Hough, M., McClure, A., Bolduc, B., Dorrepaal, E., Saleska, S., Klepac-Ceraj, V., Rich, V.
1238 (2020). Biotic and environmental drivers of plant microbiomes across a permafrost thaw
1239 gradient. Frontiers in Microbiology 11: 1-18. : <https://doi.org/10.3389/fmicb.2020.00796>
1240
1241 Huang, Y., Ciais, P., Luo, Y., Zhu, D., Wang, Y., Qiu, C., et al. (2021). Tradeoff of CO₂ and
1242 CH₄ emissions from global peatlands under water-table drawdown. Nature Climate Change
1243 11: 618-622. <https://doi.org/10.1038/s41558-021-01059-w>
1244
1245 Hugelius, G., Strauss, J., Zubrzycki, S., Harden, J. W., Schuur, E. A. G., Ping, C. L., ...
1246 Kuhry, P. (2014). Estimated stocks of circumpolar permafrost carbon with quantified
1247 uncertainty ranges and identified data gaps. Biogeosciences 11: 6573–6593.
1248 <https://doi.org/10.5194/bg-11-6573-2014>
1249
1250 Hugelius, G., Loisel, J., Chadburn, S., Jackson, R. B., Jones, M., MacDonald, G.,
1251 Marushchak, M., Olefeldt, D., Packalen, M., Siewert, M. B., Treat, C., Turetsky, M., Voigt,
1252 C., Yu, Z. (2020). Large stocks of peatland carbon and nitrogen are vulnerable to permafrost
1253 thaw. Proceedings of the National Academy of Sciences of the United States of America,
1254 117: 20438–20446. <https://doi.org/10.1073/pnas.1916387117>
1255
1256
1257 Jassey, V. E. J., Chiapusio, G., Gilbert, D., Toussaint, M. L., Binet, P. (2012).
1258 Phenoloxidase and peroxidase activities in Sphagnum-dominated peatland in a warming
1259 climate. Soil Biology and Biochemistry 46: 49–52.
1260 <https://doi.org/10.1016/j.soilbio.2011.11.011>

1261
1262 Johnston, C. E., Ewing, S. A., Harden, J. W., Varner, R. K., Wickland, K. P., Koch, J. C., et
1263 al. (2014). Effect of permafrost thaw on CO₂ and CH₄ exchange in a
1264 western Alaska peatland chronosequence. *Environmental Research Letters*
1265 9: 1-12. <https://doi.org/10.1088/1748-9326/9/8/085004>
1266
1267 Jones, M. C., Harden, J., O'Donnell, J., Manies, K., Jorgenson, T., Treat, C., Ewing, S.
1268 (2017). Rapid carbon loss and slow recovery following permafrost thaw in boreal
1269 peatlands. *Global Change Biology* 23: 1109–1127. <https://doi.org/10.1111/gcb.13403>
1270
1271 Juttonen, H., Kieman, M., Fritze, H., Hamberg, L., Laine, A. M., Merilä, P., et al. (2021).
1272 Integrating Decomposers, Methane-Cycling Microbes and Ecosystem Carbon Fluxes Along a
1273 Peatland Successional Gradient in a Land Uplift Region. *Ecosystems*.
1274 <https://doi.org/10.1007/s10021-021-00713-w>
1275
1276 Kammann, C., Grünhage, L., Jäger, H. J. (2001). A new sampling technique to monitor
1277 concentrations of CH₄, N₂O and CO₂ in air at well-defined depths in soils with varied water
1278 potential. *European Journal of Soil Science* 52: 297-303. [https://doi.org/10.1046/j.1365-](https://doi.org/10.1046/j.1365-2389.2001.00380.x)
1279 [2389.2001.00380.x](https://doi.org/10.1046/j.1365-2389.2001.00380.x)
1280
1281 Kassambara, A., Mundt, F. (2017). Package “factoextra.” R Topics Documented.
1282
1283 Kassambara, A. (2018). ggpubr: “ggplot2” Based Publication Ready Plots. R package version
1284 0.2. <https://CRAN.R-project.org/package=ggpubr>. [https://CRAN.R-](https://CRAN.R-Project.Org/Package=ggpubr)
1285 [Project.Org/Package=ggpubr](https://CRAN.R-Project.Org/Package=ggpubr). [https://doi.org/R package version 0.1.8](https://doi.org/R_package_version_0.1.8)
1286
1287 Keeling, C. D. (1958). The concentration and isotopic abundances of atmospheric carbon
1288 dioxide in rural areas. *Geochimica et Cosmochimica Acta* 13: 332-334..
1289 [https://doi.org/10.1016/0016-7037\(58\)90033-4](https://doi.org/10.1016/0016-7037(58)90033-4)
1290
1291 Kendall M.M., Boone D.R. (2006). Cultivation of methanogens from shallow marine
1292 sediments at Hydrate Ridge, Oregon. *Archaea* 2: 31-38. doi: 10.1155/2006/710190. PMID:
1293 16877319; PMCID: PMC2685590.
1294
1295 Keuper, F., van Bodegom, P.M., Dorrepaal, E., Weedon, J.T., van Hal, J., van Logtestijn, R.
1296 S.P., Aerts, R. (2012). A frozen feast: thawing permafrost increases plant-available nitrogen
1297 in subarctic peatlands. *Global Change Biology*, 18 :1998-2007. [https://doi.org/10.1111/j.1365-](https://doi.org/10.1111/j.1365-2486.2012.02663.x)
1298 [2486.2012.02663.x](https://doi.org/10.1111/j.1365-2486.2012.02663.x)
1299
1300 Keuper, F., Dorrepaal, E., van Bodegom, P.M., van Logtestijn, R., Venhuizen, G., van Hal, J.,
1301 Aerts, R. (2017). Experimentally increased nutrient availability at the permafrost thaw front
1302 selectively enhances biomass production of deep-rooting subarctic peatland species. *Global*
1303 *Change Biology* 23: 4257-4266. doi: 10.1111/gcb.13804
1304

1305 Kirkwood, J. A. H., Roy-Léveillé, P., Mykytczuk, N., Packalen, M., McLaughlin, J.,
1306 Laframboise, A., Basiliko, N. (2021). Soil Microbial Community Response to Permafrost
1307 Degradation in Palsa Fields of the Hudson Bay Lowlands: Implications for Greenhouse Gas
1308 Production in a Warming Climate. *Global Biogeochemical Cycles* 35:
1309 <https://doi.org/10.1029/2021GB006954>
1310

1311 Knoblauch, C., Beer, C., Liebner, S., Grigoriev, M.N., Pfeiffer, E.M. (2018). Methane
1312 production as key to the greenhouse gas budget of thawing permafrost. *Nature Climate*
1313 *Change* 8: 309-312. <https://doi.org/10.1038/s41558-018-0095-z>
1314

1315 Knorr, K. H., Lischeid, G., Blodau, C. (2009). Dynamics of redox processes in a
1316 minerotrophic fen exposed to a water table manipulation. *Geoderma*, 153: 379-392.
1317 <https://doi.org/10.1016/j.geoderma.2009.08.023>
1318

1319 Kotiaho, M., Fritze, H., Merilä, P. et al. (2013). Actinobacteria community structure in the
1320 peat profile of boreal bogs follows a variation in the microtopographical gradient similar to
1321 vegetation. *Plant Soil* 369: 103–114. <https://doi.org/10.1007/s11104-012-1546-3>
1322

1323 Kotsyurbenko, O. R., Friedrich, M. W., Simankova, M. V., Nozhevnikova, A. N., Golyshin,
1324 P. N., Timmis, K. N., Conrad, R. (2007). Shift from acetoclastic to H₂-dependent
1325 methanogenesis in a West Siberian peat bog at low pH values and isolation of an
1326 acidophilic *Methanobacterium* strain. *Applied and Environmental Microbiology* 73:
1327 2344–2348. <https://doi.org/10.1128/AEM.02413-06>
1328

1329 Kotsyurbenko, O.R., (2005). Trophic interactions in the methanogenic microbial community
1330 of low-temperature terrestrial ecosystems, *FEMS Microbiology Ecology* 53(3–13,
1331 <https://doi.org/10.1016/j.femsec.2004.12.009>
1332

1333 Kuhn, M., Varner, R., Bastviken, D., Crill, P., MacIntyre, S., Turetsky, M., et al. (2021).
1334 BAWLD-CH₄: A Comprehensive Dataset of Methane Fluxes from Boreal and Arctic
1335 Ecosystems. *Earth System Science Data Discussions* 13: 5151-
1336 5189. <https://doi.org/10.5194/essd-2021-141>
1337

1338 Kuhry, Peter (2008). Vegetation cover and radiocarbon dates of palsa and peat plateaus in the
1339 Hudson Bay Lowlands. *PANGAEA*, <https://doi.org/10.1594/PANGAEA.812224>,
1340 Supplement to: Kuhry, P (2008): Palsa and peat plateau development in the Hudson Bay
1341 Lowlands, Canada: timing, pathways and causes. *Boreas* 37: 316-327,
1342 <https://doi.org/10.1111/j.1502-3885.2007.00022.x>
1343

1344 Kujala, K., Seppälä, M., Holappa, T. (2008). Physical properties of peat and palsa formation.
1345 *Cold Regions Science and Technology*, 52: 408-414.
1346 <https://doi.org/10.1016/j.coldregions.2007.08.002>
1347

1348 Lee, H., Schuur, E. A. G., Inglett, K. S., Lavoie, M., Chanton, J. P. (2012). The rate of

1349 permafrost carbon release under aerobic and anaerobic conditions and its potential
1350 effects on climate. *Global Change Biology* 18: 515-527. . <https://doi.org/10.1111/j.1365->
1351 [2486.2011.02519.x](https://doi.org/10.1111/j.1365-2486.2011.02519.x)
1352
1353 Leroy, F., Gogo, S., Guimbaud, C., Bernard-Jannin, L., Hu, Z., Laggoun-Défarge, F. (2017).
1354 Vegetation composition controls temperature sensitivity of CO₂ and CH₄ emissions and
1355 DOC concentration in peatlands. *Soil Biology and Biochemistry* 107: 164-167.
1356 <https://doi.org/10.1016/j.soilbio.2017.01.005>
1357
1358 Liebner, S., Ganzert, L., Kiss, A., Yang, S., Wagner, D., Svenning, M. M. (2015). Shifts in
1359 methanogenic community composition and methane fluxes along the degradation of
1360 discontinuous permafrost. *Frontiers in Microbiology* 6: 1-10.
1361 <https://doi.org/10.3389/fmicb.2015.00356>
1362
1363 Lin, Y., Liu, D., Yuan, J., Ye, G,m Ding, W. (2017). Methanogenic community was stable in
1364 two contrasting freshwater marshes exposed to elevated atmospheric CO₂. *Frontiers in*
1365 *Microbiology* 8: 1-12. <https://doi.org/10.3389/fmicb.2017.00932>
1366
1367 Luláková, P., Perez-Mon, C., Šantrůčková, H., Ruethi, J.,Frey, B. (2019). High-alpine
1368 permafrost and active-layer soil microbiomes differ in their response to elevated
1369 temperatures. *Frontiers in Microbiology* 10: 1-16. . <https://doi.org/10.3389/fmicb.2019.00668>
1370
1371 Masella, A. P., Bartram, A. K., Truszkowski, J. M., Brown, D. G., Neufeld, J. D. (2012).
1372 PANDAseq : PAired-eND Assembler for Illumina sequences 13: 1–7.
1373 <http://www.biomedcentral.com/1471-2105/13/31>
1374
1375 McCalley, C. K., Woodcroft, B. J., Hodgkins, S. B., Wehr, R. A., Kim, E. H., Mondav, R., et
1376 al. (2014). Methane dynamics regulated by microbial community response to
1377 permafrost thaw. *Nature* 514: 478–481. <https://doi.org/10.1038/nature13798>
1378
1379 McDonald, D., Price, M.N., Goodrich, J., Nawrocki, E.P., DeSantis, T.Z., Probst, A.,
1380 Andersen, G.L., Knight, R., Hugenholtz, P. (2012). An improved Greengenes taxonomy with
1381 explicit ranks for ecological and evolutionary analyses of bacteria and archaea. *ISME*
1382 *Journal* 6: 610-618. <https://doi.org/10.1038/ismej.2011.139>
1383
1384 McNicol, G., Knox, S.H., Guilderson, T.P., Baldocchi, D.D., Silver, W.L. (2019). Where old
1385 meets new: An ecosystem study of methanogenesis in a reflooded agricultural peatland.
1386 *Global Change Biology* 26: 772-785. <https://doi.org/10.1111/gcb.14916>
1387
1388 Monteux, S., Weedon, J. T., Blume-Werry, G., Gavazov, K., Jassey, V. E. J., Johansson, M.
1389 et al. (2018). Long-term in situ permafrost thaw effects on bacterial
1390 communities and potential aerobic respiration. *ISME Journal* 12: 2129-2141.
1391 <https://doi.org/10.1038/s41396-018-0176-z>
1392

1393 Mudryk, L., Brown, R., Derksen, C., Luoju, K., Decharme, B., Helfrich, S. (2018).
1394 Surface Air Temperature [in Arctic Report Card 2018]. Retrieved from
1395 <https://www.arctic.noaa.gov/Report-Card>
1396

1397 Nielsen, C.S., Hasselquist, N.J, Nilsson, M.B., Öquist M., Järveoja J., Peichl M. (2019) .A
1398 Novel Approach for High-Frequency in-situ Quantification of Methane Oxidation in
1399 Peatlands. *Soil Systems* 3: 1-11. <https://doi.org/10.3390/soilsystems3010004>
1400

1401 Oksanen, J., Blanchet, F. G., Kindt, R., Oksanen, M. J., Suggests, M. (2013). Package
1402 ‘vegan.’ Community Ecology Package Version.
1403

1404 Olefeldt, D., Goswami, S., Grosse, G., Hayes, D., Hugelius, G., Kuhry, P., et al. (2016).
1405 Circumpolar distribution and carbon storage of thermokarst landscapes.
1406 *Nature Communications* 7:1-11. <https://doi.org/10.1038/ncomms13043>
1407

1408 Olefeldt, D., Euskirchen, E. S., Harden, J., Kane, E., McGuire, A. D., Waldrop, M. P., &
1409 Turetsky, M. R. (2017). A decade of boreal rich fen greenhouse gas fluxes in response to
1410 natural and experimental water table variability. *Global Change Biology* 23: 2428–2440.
1411 <https://doi.org/10.1111/gcb.13612>
1412

1413 Olefeldt, D., Heffernan, L., Jones, M. C., Sannel, A. B. K., Treat, C. C., & Turetsky, M. R.
1414 (2021). Permafrost thaw in northern peatlands: rapid changes in ecosystem and landscape
1415 functions. *Ecosystem Collapse and Climate Change*, 27-67.
1416

1417 Parada, A. E., Needham, D. M., Fuhrman, J. A. (2016). Every base matters: assessing
1418 small subunit rRNA primers for marine microbiomes with mock communities, time
1419 series and global field samples. *Environmental Microbiology* 18: 1403–1414.
1420 <https://doi.org/10.1111/1462-2920.13023>
1421

1422 Pelletier, N., Talbot, J., Olefeldt, D., Turetsky, M., Blodau, C., Sonnentag, O., Quinton, W. L.
1423 (2017). Influence of Holocene permafrost aggradation and thaw on the paleoecology and
1424 carbon storage of a peatland complex in northwestern Canada. *Holocene* 27: 1391–1405.
1425 <https://doi.org/10.1177/0959683617693899>
1426

1427 Perryman, C. R., McCalley, C. K., Malhotra, A., Fahnestock, M. F., Kashi, N. N., Bryce, J.
1428 G., et al. (2020). Thaw Transitions and Redox Conditions Drive Methane
1429 Oxidation in a Permafrost Peatland. *Journal of Geophysical Research: Biogeosciences*,
1430 125: 1-15.. <https://doi.org/10.1029/2019JG005526>
1431

1432 Pinheiro, J., Bates, D., DebRoy, S., Sarkar, D, et al. D.(2017). nlme: Linear and Nonlinear
1433 Mixed Effects Models. R package version 3.1-131, [https://CRAN.R-](https://CRAN.R-project.org/package=nlme)
1434 [project.org/package=nlme](https://CRAN.R-project.org/package=nlme).
1435 R Package Version 3.1-131, <https://CRAN.R-Project.Org/Package=nlme>.
1436 <https://doi.org/10.1016/j.tibs.2011.05.003>

1437
1438 Popp, T. J., Chanton, J. P., Whiting, G. J., and Grant, N. (1999), Methane stable isotope
1439 distribution at a Carex dominated fen in north central Alberta, Global Biogeochemical
1440 Cycles 13: 1063– 1077, doi:10.1029/1999GB900060.
1441
1442 Preuss, I., Knoblauch, C., Gebert, J., Pfeiffer, E.M. (2013). Improved quantification of
1443 microbial CH₄ oxidation efficiency in arctic wetland soils using carbon isotope fractionation.
1444 Biogeosciences 10: 2539-2552. <https://doi.org/10.5194/bg-10-2539-2013>
1445
1446 Quince, C., Lanzen, A., Davenport, R. J., Turnbaugh, P. J. (2011). Removing Noise From
1447 Pyrosequenced Amplicons. BMC Bioinformatics 12: 1-18. [https://doi.org/10.1186/1471-](https://doi.org/10.1186/1471-2105-12-38)
1448 [2105-12-38.](https://doi.org/10.1186/1471-2105-12-38)
1449
1450 R Core Team. (2015). R: A language and environment for statistical computing. Vienna,
1451 Austria; 2014. URL [Http://Www. R-Project. Org](http://www.R-Project.Org). Vienna, Austria: R Foundation for
1452 Statistical Computing. <https://doi.org/10.1007/978-3-540-74686-7>
1453
1454 Robroek, B. J. M., Jassey, V. E. J., Kox, M. A. R., Berendsen, R. L., Mills, R. T. E., Cécillon,
1455 L., et al. (2015). Peatland vascular plant functional types affect methane dynamics by altering
1456 microbial community structure. Journal of Ecology 103:925-934.
1457 <https://doi.org/10.1111/1365-2745.12413>
1458
1459 Robroek, B. J. M., Martí, M., Svensson, B. H., Dumont, M. G., Veraart, A. J., Jassey, V. E. J.
1460 (2021). Rewiring of peatland plant–microbe networks outpaces species turnover. Oikos 130:
1461 339-353. <https://doi.org/10.1111/oik.07635>
1462
1463 Schaefer, K., Zhang, T., Bruhwiler, L., Barrett, A. P. (2011). Amount and timing of
1464 permafrost carbon release in response to climate warming. Tellus, Series B: Chemical
1465 and Physical Meteorology 63:165-180. <https://doi.org/10.1111/j.1600-0889.2011.00527.x>
1466
1467 Schuur, E. A. G., McGuire, A. D., Schädel, C., Grosse, G., Harden, J. W., Hayes, D. J., ...
1468 Vonk, J. E. (2015). Climate change and the permafrost carbon feedback. Nature
1469 520: 171–179. <https://doi.org/10.1038/nature14338>
1470
1471 Simon, E., Canarini, A., Martin, V., Séneca, J., Böckle, T., Reinthaler, D., et al.
1472 (2020). Microbial growth and carbon use efficiency show seasonal responses in a
1473 multifactorial climate change experiment. Communications Biology 3:1-10.
1474 <https://doi.org/10.1038/s42003-020-01317-1>
1475
1476 Strack, M., Waddington, J. M., & Tuittila, E. S. (2004). Effect of water table drawdown on
1477 northern peatland methane dynamics: Implications for climate change. Global
1478 Biogeochemical Cycles 18: 1-13.. <https://doi.org/10.1029/2003GB002209>
1479

1480 Stams A.J.M., Teusink B., Sousa D.Z. (2019) Ecophysiology of Acetoclastic Methanogens.
1481 In: Stams A., Sousa D. (eds) Biogenesis of Hydrocarbons. Handbook of Hydrocarbon and
1482 Lipid Microbiology. Springer, Cham. https://doi.org/10.1007/978-3-319-78108-2_21
1483

1484 Ström, L., Ekberg, A., Mastepanov, M. and Røjle Christensen, T. (2003), The effect of
1485 vascular plants on carbon turnover and methane emissions from a tundra wetland. *Global*
1486 *Change Biology* 9: 1185-1192. <https://doi.org/10.1046/j.1365-2486.2003.00655.x>
1487

1488 Ström et al., (2012). Presence of *Eriophorum scheuchzeri* enhances substrate availability and
1489 methane emission in an Arctic wetland *Soil Biology and Biochemistry* 45: 61-70,
1490 <https://doi.org/10.1016/j.soilbio.2011.09.005>.
1491

1492 Strom, L., Falk, J.M., Skov, K., Jackowicz-Korczynski, M., Mastepanov, M., Christensen, T.,
1493 Lund, M., Schmidt, N.M. (2015). Controls of spatial and temporal variability in CH₄ flux in a
1494 high arctic fen over three years. *Biogeochemistry* 125: 21-35. [https://doi.org/10.1007/s10533-](https://doi.org/10.1007/s10533-015-0109-0)
1495 [015-0109-0](https://doi.org/10.1007/s10533-015-0109-0)
1496

1497

1498 Turetsky, M. R., Wieder, R. K., Vitt, D. H., Evans, R. J., Scott, K. D. (2007). The
1499 disappearance of relict permafrost in boreal north America: Effects on peatland carbon
1500 storage and fluxes. *Global Change Biology* 13: 1922–1934.
1501 <https://doi.org/10.1111/j.1365-2486.2007.01381.x>
1502

1503 Turetsky, Merritt R., Abbott, B. W., Jones, M. C., Anthony, K. W., Olefeldt, D., Schuur, E.
1504 A. G., et al. (2020). Carbon release through abrupt permafrost thaw.
1505 *Nature Geoscience*.13: 138-143. <https://doi.org/10.1038/s41561-019-0526-0>
1506

1507 Tuittila, E. S., Komulainen, V. M., Vasander, H., Nykanen, H., Martikainen, P. J., Laine, J.
1508 (2000). Methane dynamics of a restored cut-away peatland. *Global Change Biology*, 6: 569–
1509 581. <https://doi.org/10.1046/j.1365-2486.2000.00341.x>
1510

1511 Vanwongerghem, I., Evans, P., Parks, D. et al. (2016). Methylophilic methanogenesis
1512 discovered in the archaeal phylum Verstraetearchaeota. *Nature Microbiology* 1: 1-9.
1513 <https://doi.org/10.1038/nmicrobiol.2016.170>
1514

1515 Vishnivetskaya, T.A., Buongiorno, J., Bird, J., Krivushin, K., Spirina, E.V., Oshurkova, V.,
1516 Shcherbakova, V.A., Wilson, G., Lloyd, K.G., Rivkina, E.M. (2018). Methanogens in the
1517 Antarctic Dry Valley permafrost, *FEMS Microbiology Ecology* 94: 1-14.
1518 [fiy109, https://doi.org/10.1093/femsec/fiy109](https://doi.org/10.1093/femsec/fiy109)
1519

1520 Vitt, D. H., Halsey, L. A., Bauer, I. E., Campbell, C. (2000). Spatial and temporal trends in
1521 carbon storage of peatlands of continental western Canada through the Holocene.
1522 *Canadian Journal of Earth Sciences*, 37: 683–693. <https://doi.org/10.1139/e99-097>

1523
1524 Vitt, D. H., Halsey, L. A., Zoltai, S. C. (1994). The Bog Landforms of Continental Western
1525 Canada in Relation to Climate and Permafrost Patterns. *Arctic and Alpine Research*,
1526 26: 1-13. <https://doi.org/10.2307/1551870>
1527
1528 Weishaar, J.L., Aiken, G.R., Bergamaschi, B.A., Fram, M.S., Fujii, R., Mopper, K. (2003).
1529 Evaluation of specific ultraviolet absorbance as an indicator of the chemical composition and
1530 reactivity of dissolved organic carbon. *Environmental Science and Technology* 37: 4702-
1531 4708. <https://doi.org/10.1021/es030360x>
1532
1533 Whiticar, M. J., Faber, E., Schoell, M. (1986). Biogenic methane formation in marine and
1534 freshwater environments: CO₂ reduction vs. acetate fermentation-Isotope evidence.
1535 *Geochimica et Cosmochimica Acta*, 50: 693-709. [https://doi.org/10.1016/0016-](https://doi.org/10.1016/0016-7037(86)90346-7)
1536 [7037\(86\)90346-](https://doi.org/10.1016/0016-7037(86)90346-7)
1537 [7](https://doi.org/10.1016/0016-7037(86)90346-7)
1538
1539 Whiticar, Michael J. (1999). Carbon and hydrogen isotope systematics of bacterial formation
1540 and oxidation of methane. *Chemical Geology*, 161:291-314. [https://doi.org/10.1016/S0009-](https://doi.org/10.1016/S0009-2541(99)00092-3)
1541 [2541\(99\)00092-3](https://doi.org/10.1016/S0009-2541(99)00092-3)
1542
1543 Wickham, H. (2016). *ggplot2 -Positioning Elegant Graphics for Data Analysis*. 3rd ed.
1544 Springer-Verlag New York.
1545
1546 Wickland, K. P., Striegl, R. G., Neff, J. C., Sachs, T. (2006). Effects of permafrost melting on
1547 CO₂ and CH₄ exchange of a poorly drained black spruce lowland. *Journal of*
1548 *Geophysical Research: Biogeosciences* 111: 1–13.
1549 <https://doi.org/10.1029/2005JG000099>
1550
1551 Wüst, P.K., Horn, M.A. and Drake, H.L. (2009), Trophic links between fermenters and
1552 methanogens in a moderately acidic fen soil. *Environmental Microbiology* 11: 1395-1409.
1553 <https://doi.org/10.1111/j.1462-2920.2009.01867.x>
1554
1555 Ye, R., Jin, Q., Bohannon, B., Keller, J. K., McAllister, S. A., Bridgham, S. D. (2012). PH
1556 controls over anaerobic carbon mineralization, the efficiency of methane production, and
1557 methanogenic pathways in peatlands across an ombrotrophic-minerotrophic gradient. *Soil*
1558 *Biology and Biochemistry* 54: 36–47. <https://doi.org/10.1016/j.soilbio.2012.05.015>
1559
1560 Zhang, CJ., Pan, J., Liu, Y. et al. (2020). Genomic and transcriptomic insights into
1561 methanogenesis potential of novel methanogens from mangrove sediments. *Microbiome* 8: 1-
1562 12. <https://doi.org/10.1186/s40168-020-00876-z>
1563
1564 Zoltai, S. C. (1972). Palsas and Peat Plateaus in Central Manitoba and Saskatchewan.
1565 *Canadian Journal of Forest Research* 2: 291–302. <https://doi.org/10.1139/x72-046>
1566

1567 Zoltai, S. C. (1993). Cyclic Development of Permafrost in the Peatlands of Northwestern
1568 Alberta, Canada. *Arctic and Alpine Research* 25: 240-246.
1569 <https://doi.org/10.2307/1551820>